

Advantages of axion-like particles for the description of very-high-energy blazar spectra

Giorgio Galanti*

*Dipartimento di Fisica, Università dell'Insubria,
Via Valleggio 11, I – 22100 Como, Italy*

Marco Roncadelli[†]

INFN, Sezione di Pavia, Via A. Bassi 6, I – 27100 Pavia, Italy

Alessandro De Angelis[‡]

INFN, Sezione di Padova, Via Marzolo 8, I – 35131 Padova, Italy

Giovanni F. Bignami[§]

INAF, Viale del parco Mellini 84, I – 00136 Roma, Italy

In the last few years, the Imaging Atmospheric Cherenkov Telescopes H.E.S.S., MAGIC and VERITAS have detected more than 40 blazars in the very-high-energy range (VHE, 100 GeV – 100 TeV). During their trip to us, the VHE photons undergo an energy-dependent absorption by scattering off the infrared/optical/ultraviolet photons of the extragalactic background light (EBL), which is produced by galaxies during the whole cosmic evolution. Actually, both the observed spectra and the emitted ones predicted by conventional VHE photon emission models have a simple power-law behavior to a good approximation. Within conventional physics, the emitted slope $\Gamma_{\text{em}}(z)$ changes randomly with the source redshift z by a large amount. But, surprisingly, the $\{\Gamma_{\text{em}}(z)\}$ distribution exhibits a *correlation with z* , since the associated best-fit regression line is a *decreasing* function of z , leading blazars with harder spectra to be found *only* at larger redshift. So, how can the source distribution get to know the redshifts in such a way to adjust their $\Gamma_{\text{em}}(z)$ values so as to reproduce such a statistical correlation? It is very difficult to imagine an intrinsic mechanism which could lead to this spectral variation within conventional physics, given the fact that neither cosmological evolutionary effects nor observational selection effects can explain it. Things are quite different in the presence of axion-like particles (ALPs), which are predicted by several extensions of the Standard Model and especially by those based on superstring theories, and are attracting growing interest being also good candidates for cold dark matter. We show that photon-ALP oscillations occurring in extragalactic magnetic fields yield, for a realistic choice of the parameters, a $\{\Gamma_{\text{em}}(z)\}$ distribution whose best-fit regression line becomes amazingly *redshift-independent* – indeed in agreement with the physical intuition – and so the above problems disappear. This is evidently a highly nontrivial fact, which therefore provides preliminary evidence for the existence of ALPs. Moreover, a new scenario for VHE blazars emerges, wherein all values of $\Gamma_{\text{em}}(z)$ fall within a small strip about the horizontal best-fit regression line in the $\Gamma_{\text{em}} - z$ plane, and the large scatter of the observed values of the slope arises from the large spread of the blazar redshifts. Remarkably, this issue can be settled in the near future not only by means of astrophysical VHE data from the upcoming CTA (Cherenkov Telescope Array), HAWC (High-Altitude Water Cherenkov Observatory), GAMMA-400 (Gamma Astronomical Multifunctional Modular Apparatus), LHAASO (Large High Altitude Air Shower Observatory) and HiSCORE (Hundred Square km Cosmic Origin Explorer), but also thanks to laboratory data based on the planned experiments ALPS II (Any Light Particle Search) and IAXO (International Axion Observatory). Our Universe may in this way be offering us a compelling reason to push physics beyond the Standard Model along a very specific direction, which possibly sheds light also on the nature of cold dark matter.

PACS numbers: 14.80.Mz, 95.30.-k, 95.85.Pw, 95.85.Ry, 98.70.Rz, 98.70.Vc, 98.70.Sa

*Electronic address: gam.galanti@gmail.com

†Electronic address: marco.roncadelli@pv.infn.it

‡Electronic address: deangelis.alessandro@gmail.com

§Electronic address: giovanni.bignami@gmail.com

I. INTRODUCTION

Nearly 10 % of Active Galactic Nuclei (AGN) possess two oppositely-oriented collimated beams which emit photons up to the TeV energy range. When one of the beams is oriented towards us, the AGN is called a blazar.

Thanks to the observations carried out with the Imaging Atmospheric Cherenkov Telescopes (IACTs) like H.E.S.S. [1], MAGIC [2] and VERITAS [3], according to the Tevcat catalog 43 blazars with known redshift have been detected in the very-high-energy (VHE) range (100 GeV – 100 TeV) [4]. We stress that 40 of them are in the flaring state, whose typical lifetime ranges from a few hours to a few days. As it will explained below, 3 of them 1ES 0229+200, PKS 1441+25 and S3 0218+35 will be discarded for the sake of the present analysis.

All observed spectra of the considered VHE blazars are well fitted by a single power-law, and so they have the form $\Phi_{\text{obs}}(E_0, z) \propto K_{\text{obs},0}(z) E_0^{-\Gamma_{\text{obs}}(z)}$, where E_0 is the observed energy, while $K_{\text{obs},0}(z)$ and $\Gamma_{\text{obs}}(z)$ denote the normalization constant and the observed slope, respectively, for a source at redshift z .

Unfortunately, the observational results do not provide any *direct* information about the intrinsic properties of the sources, as the VHE gamma-ray data strongly depend on the nature of photon propagation. Indeed, according to conventional physics the blazar spectra in the VHE range are strongly affected by the presence of the Extragalactic Background Light (EBL), namely the infrared/optical/ultraviolet background photons emitted by all galaxies since their birth (for a review, see [5]). However, it should be kept in mind that if some yet-to-be-discovered new physics changes the photon propagation, then some intrinsic source properties that are currently believed to be true may actually be incorrect.

We restrict our discussion to the two standard competing models for VHE photon emission by blazars, namely the Synchrotron-Self-Compton (SSC) mechanism [6, 7] and the Hadronic Pion Production (HPP) in proton-proton scattering [8]. Both predict emitted spectra which, to a good approximation, have a single power-law behavior $\Phi_{\text{em}}(E) = K_{\text{em}} E^{-\Gamma_{\text{em}}}$ for all the considered VHE blazars, where K_{em} is the normalization constant and Γ_{em} is the emitted slope.

The relation between $\Phi_{\text{obs}}(E_0, z)$ and $\Phi_{\text{em}}(E)$ can be expressed in general terms as

$$\Phi_{\text{obs}}(E_0, z) = P_{\gamma \rightarrow \gamma}(E_0, z) \Phi_{\text{em}}(E_0(1+z)) , \quad (1)$$

where $P_{\gamma \rightarrow \gamma}(E_0, z)$ is the photon survival probability from the source to us, and is usually written in terms of the optical depth $\tau_{\gamma}(E_0, z)$ as

$$P_{\gamma \rightarrow \gamma}(E_0, z) = e^{-\tau_{\gamma}(E_0, z)} . \quad (2)$$

Before proceeding, a remark is compelling. A few years ago, a radically different mechanism has been put forward in order to explain the IACT observations. Basically, the idea is that *protons* are accelerated inside blazars up to energies of order 10^{11} GeV, while VHE emitted photons are neglected altogether. When the proton distance from the Galaxy is in the range 10 – 100 Mpc, they scatter off EBL photons through the process $p + \gamma \rightarrow p + \pi^0$, so that the immediate decays $\pi^0 \rightarrow \gamma + \gamma$ produce an electromagnetic shower of secondary photons: it is *these photons* that replace the emitted photons in such a scenario [9]. Two characteristic features of this mechanism should be stressed in connection with the present analysis.

- It is expected this effect to be important for sources at redshifts $z > 0.15$ and energies $E_0 > 1$ TeV [10].
- Observed blazars variability shorter than 0.1 yr can be explained only for $z > 0.20$ at $E_0 > 1$ TeV [10].

Now, a glance at the values of z for the considered sources reported in Table III shows that we have 28 blazars with $z < 0.15$, and so – owing to the first item – these blazars cannot be explained by the mechanism in question. Let us next turn to the issue of variability. The overwhelming majority of the sources considered here are flaring, with a lifetime typically ranging from a few hours to a few days. Only the blazars 1ES 0229+200, 1ES 0806+524 and 1ES 1101-232 have a constant γ -ray luminosity [11]. A look at the energy range ΔE_0 over which each source is observed (reported in Table III) shows that the lowest values of E_0 are much below 1 TeV (with one exception to be addressed below). Because the shapes of the observed spectra do not exhibit any peculiar feature, it is evident that a *single* blazar is explained by the a *single mechanism*, and so we must conclude that the considered approach can explain at most 3 sources. Thus, here we do not address such an alternative possibility – whose relevance can become important at much larger energies – up to an exception. An analysis of the properties of the blazar 1ES 0229+200 has shown that it can hardly be explained by the SSC mechanism. Moreover, since its VHE luminosity is constant, this source is more likely to be explained by the proton emission model [12]. For this reason, we discard it from our discussion.

The main issue we are concerned with in this paper is a possible correlation between the distribution of blazar VHE *emitted spectra* and the *redshift*.

Superficially, the reader might well wonder about such a question. Why should a correlation of this kind exist? Cosmological evolutionary effects are certainly harmless out to redshift $z \simeq 0.5$, and when observational selection biases are properly taken into account no such a correlation is expected to show up. As we shall see, this is not the case, and it is indeed this fact that has prompted our analysis.

We are now in position to outline the structure of the paper. In Section II we report all observational information needed for the present analysis. Section III is devoted to inferring for each considered source the emitted slope $\Gamma_{\text{em}}^{\text{CP}}(z)$ and the emitted flux normalization $K_{\text{em}}^{\text{CP}}(z)$ starting from the observed ones $\Gamma_{\text{obs}}(z)$ and $K_{\text{obs},0}(z)$ assuming conventional physics, namely taking into account the effect of the EBL absorption alone. We next plot the values of $\Gamma_{\text{em}}^{\text{CP}}(z)$ and $K_{\text{em}}^{\text{CP}}(z)$ as a function of redshift z for all considered blazars. After performing a statistical analysis of the $\{\Gamma_{\text{em}}^{\text{CP}}(z)\}$ distribution, we end up with the conclusion that the resulting best-fit regression line *decreases with increasing redshift*. While this trend might be interpreted as an observational selection effect, a deeper scrutiny based on observational information shows that this is by no means the case. So, we are led to the conclusion that such a behavior is at odd with physical intuition, which would instead demand the best-fit regression line to be redshift-independent. In Section IV we try to fit the same data in the $\Gamma_{\text{em}}^{\text{CP}} - z$ plane with a horizontal straight line, but we conclude that it does not work. As an attempt to achieve a physically satisfactory scenario, in Section V we introduce Axion-Like Particles (ALP) (for a review, see [13]). They are spin-zero, neutral and extremely light pseudo-scalar bosons predicted by several extensions of the Standard Model of particle physics, and especially by those based on superstring theories [14–23]. They interact only with two photons. Depending on their mass and two-photon coupling, they can be quite good candidates for cold dark matter [24] and give rise to very interesting astrophysical effects (to be discussed in Section VI), so that nowadays ALPs are attracting growing interest. Specifically, we suppose that photon-ALP oscillations take place in extragalactic magnetic fields of strength about 0.1 nG – in agreement with the predictions of the galactic outflows models [25, 26] – as first proposed in [27]. As a consequence, photon propagation gets affected by EBL as well as by photon-ALP oscillations, whose combined effect is to *substantially reduce* the cosmic opacity brought about by the EBL alone, thereby considerably widening the conventional γ -ray horizon [28]. Accordingly, we re-derive for every source the emitted slope $\Gamma_{\text{em}}^{\text{ALP}}(z)$ and the emitted flux normalization $K_{\text{em}}^{\text{ALP}}(z)$ starting from the observed ones $\Gamma_{\text{obs}}(z)$ and $K_{\text{obs},0}(z)$. Proceeding as before, we plot again the values of $\Gamma_{\text{em}}^{\text{ALP}}(z)$ and $K_{\text{em}}^{\text{ALP}}(z)$ as a function of redshift z for all considered sources. A statistical

analysis of the $\{\Gamma_{\text{em}}^{\text{ALP}}(z)\}$ distribution now shows that for a realistic choice of the parameters the corresponding best-fit regression line turns out to be indeed *independent* of redshift. Moreover, the values of $\Gamma_{\text{em}}^{\text{ALP}}(z)$ for the individual blazars exhibit a small scatter about such a best-fit straight regression line. We stress that the fact that the best-fit regression becomes a straight line horizontal in the $\Gamma_{\text{em}}^{\text{ALP}} - z$ plane is an amazing fact, which is the only one in agreement with physical intuition and provides a strong hint of the existence of ALPs. Finally, in Section VI we briefly discuss a new view of VHE blazars emerging from our result, its relevance – also in connection with other VHE astrophysical achievements employing ALPs – and its implications for the future of VHE astrophysics. Finally, in order to avoid breaking the main line of thought by somewhat involved technicalities concerning the evaluation of the photon survival probability in the presence of ALPs, we report this matter in the Appendix.

II. OBSERVATIONAL INFORMATION

The observational quantities concerning every blazar which are relevant for the present analysis are: the redshift z , the observed flux $\Phi_{\text{obs}}(E_0, z)$ and the energy range ΔE_0 where each source is observed.

Some care should be paid to the normalization constant entering the expression of $\Phi_{\text{obs}}(E_0, z)$, which is usually written as

$$\Phi_{\text{obs}}(E_0, z) = K_{\text{obs},0}(z) \left(\frac{E_0}{E_{\text{ref}}} \right)^{-\Gamma_{\text{obs}}(z)}, \quad (3)$$

where E_{ref} is an arbitrary energy value needed to make the exponential dimensionless, and in general *varies* from source to source. Manifestly, for the sake of comparison among the flux normalization constants for the different sources we have to recast Eq. (3) into a form such that E_{ref} gets replaced by a quantity which is equal for all sources. Choosing as a fiducial normalization energy 300 GeV, it amounts to defining the new normalization constant as

$$K_{\text{obs}}(z) \equiv K_{\text{obs},0}(z) \left(\frac{300 \text{ GeV}}{E_{\text{ref}}} \right)^{-\Gamma_{\text{obs}}(z)}, \quad (4)$$

so that Eq. (3) becomes

$$\Phi_{\text{obs}}(E_0, z) = K_{\text{obs}}(z) \left(\frac{E_0}{300 \text{ GeV}} \right)^{-\Gamma_{\text{obs}}(z)}. \quad (5)$$

Note that we have $\Phi_{\text{obs}}(300 \text{ GeV}, z) = K_{\text{obs}}(z)$. Henceforth, we shall deal exclusively with the values of $K_{\text{obs}}(z)$. Therefore, we need to know both $K_{\text{obs}}(z)$ and $\Gamma_{\text{obs}}(z)$ for any source.

The values of z , $\Gamma_{\text{obs}}(z)$, ΔE_0 and $K_{\text{obs}}(z)$ for all considered blazars are reported in Table III. Observe that while the error bars associated with $\Gamma_{\text{obs}}(z)$ are quoted, those referring to $K_{\text{obs}}(z)$ are not because of their lack in many of the published papers, but for our consideration this is not a big problem (nevertheless, the reader should keep this point in mind throughout the paper). The observed slope Γ_{obs} and the normalization constant K_{obs} as a function of z are plotted in the left and right panels of Fig. 1, respectively.

Finally, denoting by N_{obs} the total number of detected photons per unit time, since $\Phi_{\text{obs}}(E_0, z) = dN_{\text{obs}}/(dE_0 dA)$ it follows that observed γ -ray luminosity per unit area $F_{\text{obs},\Delta E_0}(z)$ is the integral of $\Phi_{\text{obs}}(E_0, z)$ over ΔE_0 .

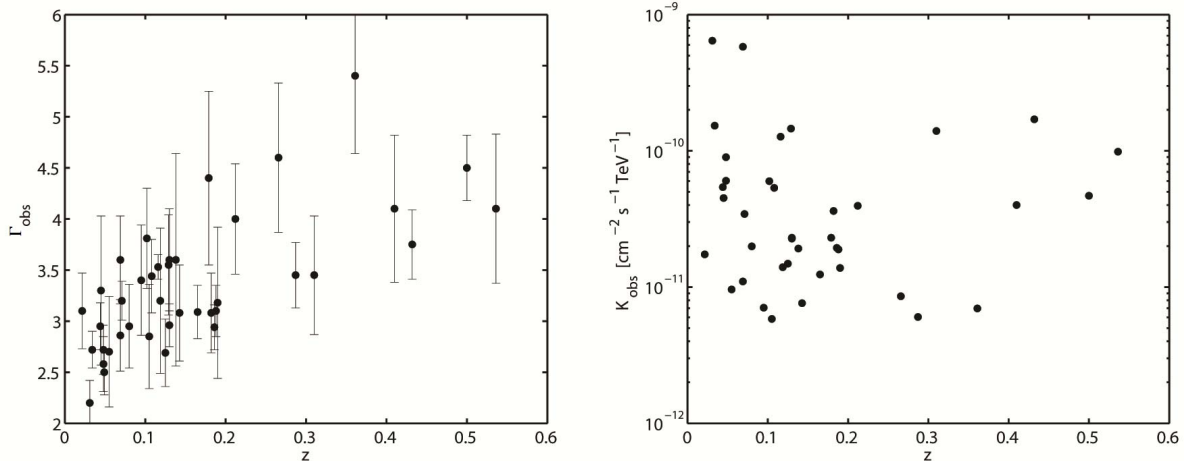


FIG. 1: *Left panel:* The values of the slope Γ_{obs} are plotted versus the source redshift z for all considered blazars. *Right panel:* The values of the normalization constant K_{obs} are similarly plotted versus the source redshift z for the same blazars in the left panel.

III. CONVENTIONAL PROPAGATION IN EXTRAGALACTIC SPACE

After a long period of uncertainty on the EBL precise spectral energy distribution and photon number density, today a convergence seems to be reached [5], well represented e.g. by the model of Franceschini, Rodighiero and Vaccari (FRV) [29], which we use for convenience.

Owing to $\gamma\gamma \rightarrow e^+e^-$ scattering off EBL photons [30, 31], the emitted VHE photons undergo an energy-dependent absorption, so that the VHE photon survival probability is given by Eq. (2) with $\tau_\gamma(E_0, z) \rightarrow \tau_\gamma^{\text{FRV}}(E_0, z)$, where $\tau_\gamma^{\text{FRV}}(E_0, z)$ is the optical depth of the EBL as evaluated within the FRV model in a standard fashion using the photon spectral number density [32–34]. As a consequence, the observed flux $\Phi_{\text{obs}}(E_0, z)$ is related to the emitted one $\Phi_{\text{em}}^{\text{CP}}(E)$ by

$$\Phi_{\text{obs}}(E_0, z) = e^{-\tau_\gamma^{\text{FRV}}(E_0, z)} \Phi_{\text{em}}^{\text{CP}}(E_0(1+z)). \quad (6)$$

Let us begin by deriving the emitted spectrum of every source, starting from the observed one, within conventional physics. As a preliminary step, we rewrite Eq. (6) as

$$\Phi_{\text{em}}^{\text{CP}}(E_0(1+z)) = e^{\tau_\gamma^{\text{FRV}}(E_0, z)} K_{\text{obs}}(z) \left(\frac{E_0}{300 \text{ GeV}} \right)^{-\Gamma_{\text{obs}}(z)}. \quad (7)$$

Owing to the presence of the exponential in the r.h.s. of Eq. (7), $\Phi_{\text{em}}^{\text{CP}}(E_0(1+z))$ cannot behave as an exact power law (unless $\tau_\gamma^{\text{FRV}}(E_0, z)$ has a pure logarithmic z -dependence). Yet, we have pointed out that it is expected to be close to it. So, we best-fit $\Phi_{\text{em}}^{\text{CP}}(E_0(1+z))$ in Eq. (7) to the single power-law expression

$$\Phi_{\text{em}}^{\text{CP,BF}}(E_0(1+z)) = K_{\text{em}}^{\text{CP}}(z) \left(\frac{(1+z)E_0}{300 \text{ GeV}} \right)^{-\Gamma_{\text{em}}^{\text{CP}}(z)} \quad (8)$$

over the energy range ΔE_0 where the source is observed. Incidentally, we neglect error bars in the values of $\tau_\gamma^{\text{FRV}}(E_0, z)$ because they are not quoted by FRV. Since $\Gamma_{\text{em}}^{\text{CP}}(z)$ depends linearly on $\Gamma_{\text{obs}}(z)$, the inferred values of $\Gamma_{\text{em}}^{\text{CP}}(z)$ have the same error bars as the values of $\Gamma_{\text{obs}}(z)$ quoted in Table III.

Of course, we are well aware that the best procedure would be to de-absorb each bin of the observed spectrum, thereby getting the emitted spectrum and next applying to it the above best-fitting procedure. Unfortunately, such a strategy is not viable in practice because the single observed energy bins with related error bars are not available from published papers. Nevertheless, the difference between the two procedures is expected to be relevant only for those sources whose highest energy points are affected by a large uncertainty, like 1ES 0229+200 – observed up to about 11 TeV – which is however discarded.

The values of the emitted slope $\Gamma_{\text{em}}^{\text{CP}}(z)$ are reported in Table IV and plotted in the left panel of Fig. 2. Similarly, the values of the normalization constant $K_{\text{em}}^{\text{CP}}(z)$ are listed in Table VI and plotted in the right panel of Fig. 2. Again, denoting by N_{em} the total number of emitted photons per unit time, because $\Phi_{\text{em}}(E, z) = dN_{\text{em}}/(dE dA)$, we see – similarly as before – that the emitted γ -ray luminosity per unit area $F_{\text{em}, \Delta E}^{\text{CP}}(z)$ is the integral of $\Phi_{\text{em}}(E, z)$ over ΔE , whose values are reported in Table VII.

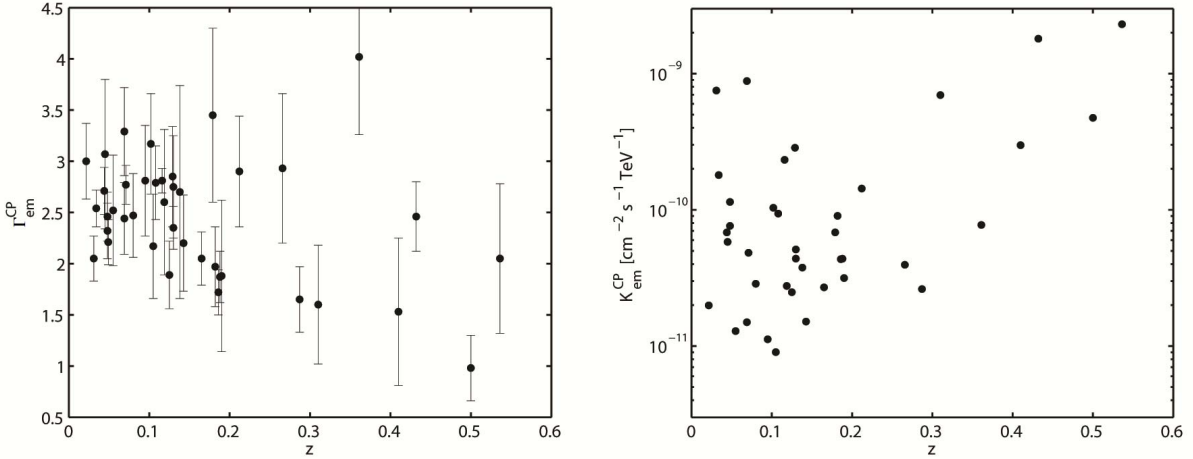


FIG. 2: *Left panel:* The values of the slope $\Gamma_{\text{em}}^{\text{CP}}$ are plotted versus the source redshift z for all considered blazars. *Right panel:* The values of the normalization constant $K_{\text{em}}^{\text{CP}}$ are similarly plotted versus the source redshift z for the same blazars in the left panel.

We proceed by performing a statistical analysis of all values of $\Gamma_{\text{em}}^{\text{CP}}(z)$ as a function of z . Specifically, we use the least square method and try to fit the data with one parameter (horizontal straight line), two parameters (first-order polynomial), and three parameters (second-order polynomial). In order to test the statistical significance of the fits we evaluate the corresponding χ_{red}^2 . The values of the χ_{red}^2 obtained for the three fits are $\chi_{\text{red}}^2 = 2.35$, $\chi_{\text{red}}^2 = 1.83$ and $\chi_{\text{red}}^2 = 1.87$, respectively. Thus, data appear to be best-fitted by the first-order polynomial

$$\Gamma_{\text{em}}^{\text{CP}}(z) = 2.68 - 2.21 z . \quad (9)$$

The of $\{\Gamma_{\text{em}}^{\text{CP}}\}$ distribution as a function of z and the associated best-fit straight regression line as defined by the last equation are plotted in Fig. 3.

We stress that in order to appreciate the physical meaning of the best-fit straight regression line in question we should recall that $\Gamma_{\text{em}}^{\text{CP}}(z)$ is the *exponent* of the emitted energy entering $\Phi_{\text{em}}^{\text{CP}}(E)$. Hence, in the two extreme cases we have

$$\Phi_{\text{em}}^{\text{CP}}(E, 0) \propto E^{-2.68} , \quad \Phi_{\text{em}}^{\text{CP}}(E, 0.6) \propto E^{-1.35} , \quad (10)$$

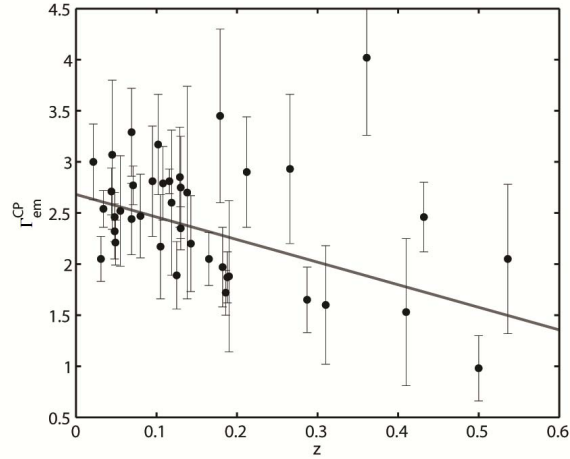


FIG. 3: Same as the left panel of Fig. 2 but with superimposed the best-fit straight regression line given by Eq. 9.

thereby implying that its nonvanishing slope gives rise to a *large variation* of the emitted flux with redshift.

Actually, one of the effects of the obtained best-fit straight regression line is that blazars with harder spectra are found *only* at larger redshift. What is the *physical meaning* of this fact?

Since we have intentionally neglected the two blazars PKS 1441+25 and S3 0218+35 both at $z \simeq 0.94$, our set of sources extends up to $z \simeq 0.54$ (3C 279). Therefore, we are concerned with a relatively local sample, and so cosmological evolutionary effects are insignificant.

Let us proceed to address all possible observational selection biases.

- As we look at larger distances only the brighter sources are observed while the fainter ones progressively disappear.
- Looking at greater distances entails that larger regions of space are probed, and so – under the assumption of an uniform source distribution – a larger number of brighter blazars should be detected. Now, the physical explanation of the best-fit straight regression line in Fig. 3 would naturally arise provided that $F_{\text{em},\Delta E}^{\text{CP}}(z)$ *tightly correlates* with $\Gamma_{\text{em}}^{\text{CP}}(z)$ in such a way that *brighter sources have harder spectra*. Then the above selection bias translates into the statement that looking at greater distances implies that a larger number of blazars with harder spectra should be observed, which is just what Fig. 3 tells us. So, the real question concerns the existence of a tight correlation between $F_{\text{em},\Delta E}^{\text{CP}}(z)$ and $\Gamma_{\text{em}}^{\text{CP}}(z)$.
- Similarly, a logically consistent possibility would be that the jet opening angle $\delta(z)$ were *tightly correlated* with $\Gamma_{\text{em}}^{\text{CP}}(z)$ so that sources with stronger beaming had harder spectra: in such a situation – under the previous assumption of an uniform source distribution – the probability that the beam points towards us increases as larger regions of space are probed, and so sources with harder spectra would be more copiously found at larger distances, again in agreement with what Fig. 3 entails.

In order to get a deeper insight into the issue addressed in the second item, we proceed by plotting $F_{\text{em},\Delta E}^{\text{CP}}$ versus $\Gamma_{\text{em}}^{\text{CP}}$ in Fig. 4. We see that $F_{\text{em},\Delta E}^{\text{CP}}$ and $\Gamma_{\text{em}}^{\text{CP}}$ are *totally uncorrelated*. As

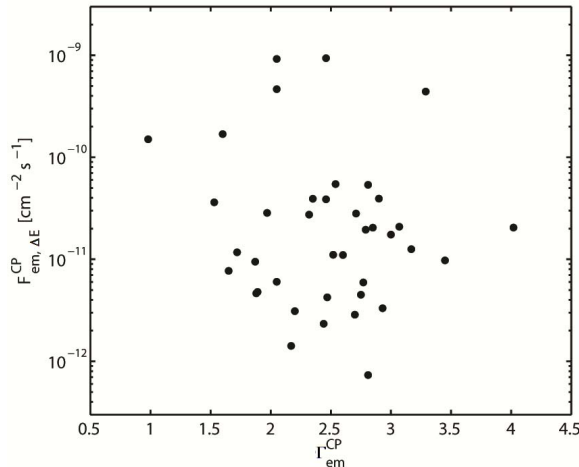


FIG. 4: $F_{em, \Delta E}^{CP}$ is plotted versus Γ_{em}^{CP} .

a consequence, the cheap explanation outlined in the second item concerning the behavior of the best-fit straight regression line in Fig. 3 is doomed to failure.

Finally, the possibility contemplated in the third item can also be excluded very easily by comparing the values of $\Gamma_{em}^{CP}(z)$ as reported in Table IV with those estimated for $\delta(z)$ in [35]. What turns out is that no correlation whatsoever between $\delta(z)$ and $\Gamma_{em}^{CP}(z)$ exists.

It is very difficult to imagine an intrinsic mechanism which could explain the best-fit straight regression line in Fig. 3 in a physically satisfactory way within conventional physics. Otherwise stated, how can a source get to know its redshift z in such a way to adjust its emitted slope $\Gamma_{em}^{CP}(z)$ so as to reproduce the distribution with best-fit straight regression line reported in Fig. 3?

We are therefore led to regard the situation emerging from the above discussion as in manifest disagreement with physical intuition, which would instead demand the best-fit straight regression line to be *horizontal* in the $\Gamma_{em}^{CP} - z$ plane.

IV. AN ATTEMPT BASED ON CONVENTIONAL PHYSICS

In spite of our previous finding, let us nevertheless try to *impose by hand* that the same data set $\{\Gamma_{em}^{CP}(z)\}$ considered before is fitted by a horizontal straight line, and see what happens. The result is exhibited in Fig. 5. In this case, we have $\Gamma_{em}^{CP} = 2.41$ and $\chi_{red}^2 = 2.35$.

Manifestly, this scenario does not work, since the value of χ_{red}^2 is unduly large. This fact hardly comes as a surprise, since we are not best-fitting the data. Still, this is a useful exercise, since it quantifies the price we have to pay in order to have a horizontal fitting straight line within conventional physics, and will be a benchmark for comparison when the ALP scenario will be considered.

Much for the same reason, it is instructive to encompass 95% of the observed sources inside a strip centered on the horizontal fitting line $\Gamma_{em}^{CP} = 2.41$. What is its width $\Delta\Gamma_{em}^{CP}$? The answer is $\Delta\Gamma_{em}^{CP} = 0.94$, which is 39% of the value $\Gamma_{em}^{CP} = 2.41$.

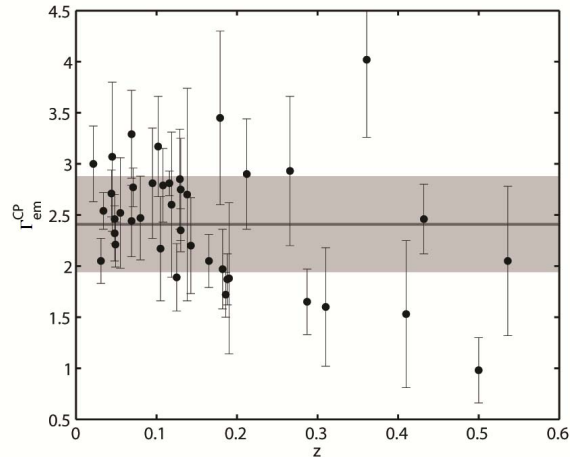


FIG. 5: Horizontal fitting straight line in conventional physics. The values of $\Gamma_{\text{em}}^{\text{CP}}$ are plotted versus the source redshift z for all considered blazars with the corresponding error bars. Superimposed is the horizontal fitting straight line $\Gamma_{\text{em}}^{\text{CP}} = 2.41$ with $\chi_{\text{red}}^2 = 2.35$. The grey strip encompasses 95% of the sources and its width is $\Delta\Gamma_{\text{em}}^{\text{CP}} = 0.94$, which equals 39% of the value $\Gamma_{\text{em}}^{\text{CP}} = 2.41$.

V. AN ATTEMPT BASED ON AXION-LIKE PARTICLES

As an alternative possibility to achieve a physically satisfactory situation, we invoke new physics in the form of axion-like particles (ALPs). As discussed in the Appendix, their most characteristic feature is to couple only to two photons with a coupling constant $g_{a\gamma\gamma}$ according to the Feynman diagram shown in Fig. 6. Clearly, in the presence of the extragalactic magnetic field \mathbf{B} one photon line in Fig. 6 represents the \mathbf{B} field, and so we see that in such a situation energy-conserving oscillations between VHE photons and ALPs take place [27]. Accordingly, photons acquire a split personality, traveling for some time as real photons – which suffer EBL absorption – and for some time as ALPs, which are unaffected by the EBL (as explicitly shown in the Appendix). As a consequence, $\tau_{\gamma}(E_0, z)$ gets replaced by the effective optical depth $\tau_{\gamma}^{\text{eff}}(E_0, z)$, which is manifestly *smaller* than $\tau_{\gamma}(E_0, z)$ and is a monotonically increasing function of E_0 and z . The crux of the argument is that since the photon survival probability is now $P_{\gamma \rightarrow \gamma}^{\text{ALP}}(E_0, z) = e^{-\tau_{\gamma}^{\text{eff}}(E_0, z)}$, even a *small* decrease of $\tau_{\gamma}^{\text{eff}}(E_0, z)$ with respect to $\tau_{\gamma}^{\text{FRV}}(E_0, z)$ gives rise to a *large* increase of the photon survival probability, as compared to the case of conventional physics. So, the main consequence of photon-ALP oscillations is to *substantially attenuate* the EBL absorption and consequently to considerably enlarging the conventional γ -ray horizon [28].

Actually, $P_{\gamma \rightarrow \gamma}^{\text{ALP}}(E_0, z)$ can be computed exactly as outlined in the Appendix, where it is explained that the extragalactic magnetic field likely has a domain-like structure (at least in first approximation), namely that \mathbf{B} is homogeneous over a domain of size L_{dom} and has approximately the same strength B in all domains, but its direction randomly changes from one domain to the next [37–39] (more about this, in the Appendix). Furthermore, it will be shown that the considered ALP scenario contains only two free parameters $\xi \propto g_{a\gamma\gamma} B$ and L_{dom} : they obviously show up in $P_{\gamma \rightarrow \gamma}^{\text{ALP}}(E_0, z)$ even though such a dependence is not explicitly exhibited for notational simplicity. Realistic values of these parameters are $\xi = 0.1, 0.5, 1, 5$ and $L_{\text{dom}} = 4 \text{ Mpc}, 10 \text{ Mpc}$, which will be regarded as our benchmark values. In reality, a third free parameter is the ALP mass m , but we assume $m < 10^{-9} \text{ eV}$ which entails that $P_{\gamma \rightarrow \gamma}^{\text{ALP}}(E_0, z)$ is *independent* of m (as discussed in the Appendix).

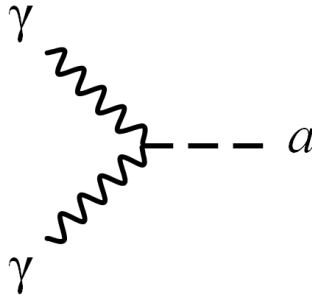


FIG. 6: Feynman diagram for the two-photon ALP coupling.

At this point, knowing $P_{\gamma \rightarrow \gamma}^{\text{ALP}}(E_0, z)$, we proceed as above. To wit, we first write the emitted flux of every source as

$$\Phi_{\text{em}}^{\text{ALP}}(E_0(1+z)) = \left(P_{\gamma \rightarrow \gamma}^{\text{ALP}}(E_0, z) \right)^{-1} K_{\text{obs}}(z) \left(\frac{E_0}{300 \text{ GeV}} \right)^{-\Gamma_{\text{obs}}(z)}. \quad (11)$$

Next, we best-fit $\Phi_{\text{em}}^{\text{ALP}}(E_0(1+z))$ in Eq. (11) to the single power-law expression

$$\Phi_{\text{em}}^{\text{ALP,BF}}(E_0(1+z)) = K_{\text{em}}^{\text{ALP}}(z) \left(\frac{(1+z)E_0}{300 \text{ GeV}} \right)^{-\Gamma_{\text{em}}^{\text{ALP}}(z)} \quad (12)$$

over the energy range ΔE_0 where the source is observed. It goes without saying that the remarks just below Eq. (8) apply here as well.

This procedure is performed for each benchmark value of ξ and L_{dom} . We report in Table IV the values of $\Gamma_{\text{em}}^{\text{ALP}}(z)$ for $L_{\text{dom}} = 4 \text{ Mpc}$, $\xi = 0.1, 0.5, 1, 5$, and similarly Table V contains the values of $\Gamma_{\text{em}}^{\text{ALP}}(z)$ for $L_{\text{dom}} = 10 \text{ Mpc}$, $\xi = 0.1, 0.5, 1, 5$.

We can at this point carry out a statistical analysis of the values of $\Gamma_{\text{em}}^{\text{ALP}}(z)$ as a function of z , again for any benchmark value of ξ and L_{dom} . We still use the least square method and we try to fit the data with one parameter (horizontal line), two parameters (first-order polynomial) and three parameters (second-order polynomial). Finally, in order to quantify the statistical significance of each fit we compute the χ_{red}^2 , whose values are reported in Table I for $L_{\text{dom}} = 4 \text{ Mpc}$, $\xi = 0.1, 0.5, 1, 5$, and in Table II for $L_{\text{dom}} = 10 \text{ Mpc}$, $\xi = 0.1, 0.5, 1, 5$.

# of fit parameters	$\chi_{\text{red,CP}}^2$	$\chi_{\text{red,ALP}}^2$			
		$\xi = 0.1$	$\xi = 0.5$	$\xi = 1$	$\xi = 5$
1	2.35	2.26	1.43	1.45	1.55
2	1.83	1.79	1.46	1.48	1.57
3	1.87	1.84	1.48	1.51	1.60

TABLE I: The values of χ_{red}^2 are displayed for the three fitting models considered in the text. In the first column the number of parameters in each fitting model is reported. The second column concerns deabsorption according to conventional physics, using the EBL model of FRV. The other columns pertain to the photon-ALP oscillation scenario with the EBL still described by the FRV model, and exhibit the values of χ_{red}^2 for $L_{\text{dom}} = 4 \text{ Mpc}$ and different choices of ξ . The value in bold-face is the minimum of χ_{red}^2 .

# of fit parameters	$\chi_{\text{red,CP}}^2$	$\chi_{\text{red,ALP}}^2$			
		$\xi = 0.1$	$\xi = 0.5$	$\xi = 1$	$\xi = 5$
1	2.35	2.05	1.39	1.51	1.55
2	1.83	1.72	1.43	1.54	1.57
3	1.87	1.77	1.47	1.57	1.60

TABLE II: Same as Table I, but with $L_{\text{dom}} = 10$ Mpc. The value in bold-face is the minimum of χ_{red}^2 .

Hence, we see that the best-fitting procedure singles out the two following preferred cases.

- $L_{\text{dom}} = 4$ Mpc, $\xi = 0.5$, the *horizontal* straight regression line with equation $\Gamma_{\text{em}}^{\text{ALP}} = 2.52$ and $\chi_{\text{red,ALP}}^2 = 1.43$.
- $L_{\text{dom}} = 10$ Mpc, $\xi = 0.5$, the *horizontal* straight regression line with equation $\Gamma_{\text{em}}^{\text{ALP}} = 2.58$ and $\chi_{\text{red,ALP}}^2 = 1.39$.

For simplicity, only for the two preferred cases are the values of $\Gamma_{\text{em}}^{\text{ALP}}(z)$ plotted in the left panels of Fig. 7. Also, only for these two cases are the values of $K_{\text{em}}^{\text{ALP}}(z)$ reported in Table VI and plotted in the right panels of Fig. 7.

Clearly, for any choice of L_{dom} the best-fitting procedure fixes the values of ξ and $\chi_{\text{red,ALP}}^2$. Even though we have taken realistic values for L_{dom} , in the absence of any information about its actual value it can well happen that other interesting results can emerge for different values of L_{dom} .

Let us summarize somewhat schematically the main achievements offered by the present scenario, especially emphasizing analogies and differences with respect to the situation based on conventional physics (considered in Sections III and IV).

- The existence of an ALP with mass $m < 10^{-9}$ eV and suitable realistic values of the parameters – such as $\xi = 0.5$ and $L_{\text{dom}} = 4$ Mpc or $L_{\text{dom}} = 10$ Mpc – gives rise to sizable photon-ALP oscillations in extragalactic space and yields a best-fit straight regression line for the $\{\Gamma_{\text{em}}^{\text{ALP}}(z)\}$ distribution which is just *horizontal*, in perfect agreement with the expectation based on physical intuition. We stress that this is an *automatic* consequence of the present model, and not an *ad hoc* requirement as in the case discussed in Section IV. The situation is illustrated in the left panels of Fig. 7.
- The lack of correlation between $F_{\text{em},\Delta E}$ and Γ_{em} found in the context of conventional physics remains true in the presence of photon-ALP oscillations, thereby implying that again observational selection biases play no rôle. This is shown in Fig. 9.
- A look at Table VII shows that the values of $F_{\text{em},\Delta E}^{\text{ALP}}$ are systematically slightly larger than those of $F_{\text{em},\Delta E}^{\text{CP}}$. This fact is in line with our expectations, and the reason is as follows. Since the values of $F_{\text{obs},\Delta E}$ are obviously fixed, such a difference has to be due to the photon propagation in the presence of photon-ALP oscillations and is the result of two competing effects. One of them is that at energies slightly larger than 100 GeV the EBL absorption is negligible. Accordingly, in the presence of many magnetic domains (as in the considered situation) it is well known that the emitted photon flux gets reduced by a factor 1/3, due to the equipartition among the three degrees of freedom (2 photon polarization states and 1 ALP state), thereby producing a dimming of the source as compared to conventional physics [36]. The other effect occurs at larger energies, where EBL absorption becomes

important. Correspondingly, photon-ALP oscillation enhance the observed photon flux as compared to conventional physics, but since the emitted photon flux is larger at lower energies, $F_{\text{em},\Delta E}^{\text{ALP}}$ has to be larger than $F_{\text{em},\Delta E}^{\text{CP}}$ in order to produce the same $F_{\text{obs},\Delta E}$.

- As in Section IV, it is interesting to compute the width $\Delta\Gamma_{\text{em}}^{\text{ALP}}$ of the strip – centered on the best-fit straight regression line $\Gamma_{\text{em}}^{\text{ALP}}$ – which encompasses 95% of the considered blazars. We find $\Delta\Gamma_{\text{em}}^{\text{ALP}} = 0.70$ which is 28% of the value $\Gamma_{\text{em}}^{\text{ALP}} = 2.52$ for $L_{\text{dom}} = 4$ Mpc, and $\Delta\Gamma_{\text{em}}^{\text{ALP}} = 0.60$ which is 23% of the value $\Gamma_{\text{em}}^{\text{ALP}} = 2.58$ for $L_{\text{dom}} = 10$ Mpc. These widths are considerably smaller than what we found within conventional physics in Section IV, namely $\Delta\Gamma_{\text{em}}^{\text{CP}} = 0.94$.

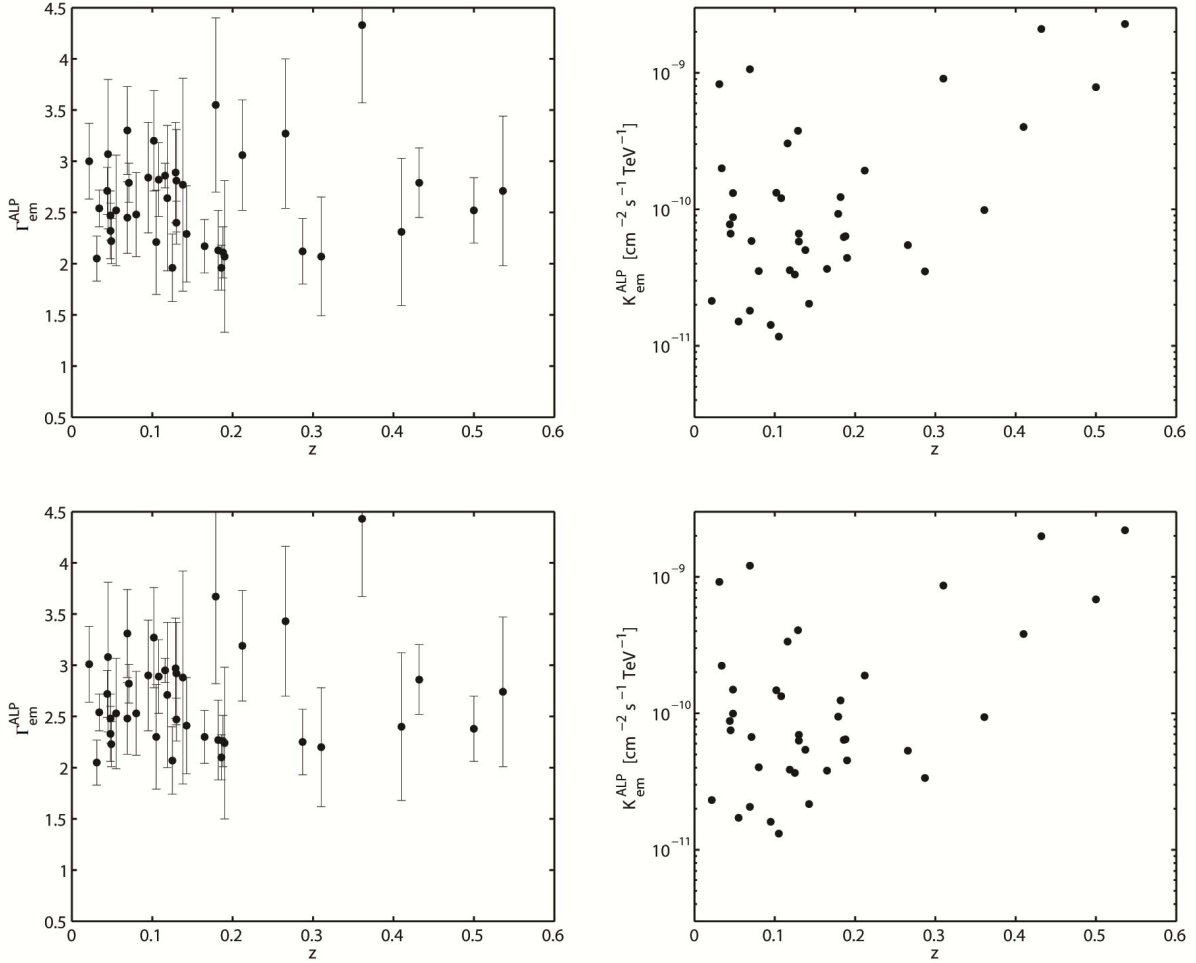


FIG. 7: *Left panels:* The values of the slope $\Gamma_{\text{em}}^{\text{ALP}}$ are plotted versus the source redshift z for all considered blazars. *Right panels:* The values of the normalization constant $K_{\text{em}}^{\text{ALP}}$ are similarly plotted versus the source redshift z for the same blazars in the left panels. The *upper row* refers to the case $\xi = 0.5$ and $L_{\text{dom}} = 4$ Mpc, while the *lower row* to the case $\xi = 0.5$ and $L_{\text{dom}} = 10$ Mpc.

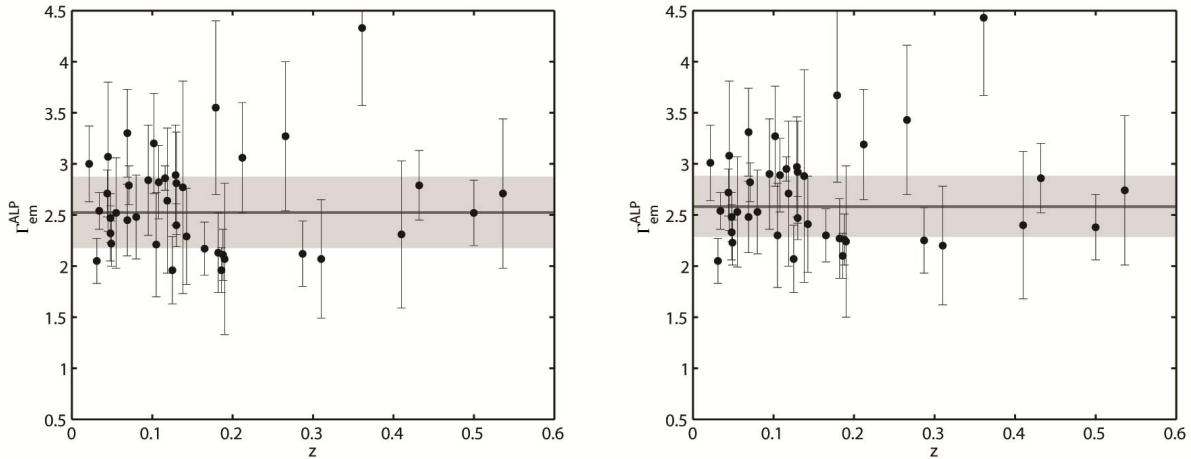


FIG. 8: Same as the left panels of Fig. 7 but with superimposed the best-fit horizontal straight regression line. Moreover, in either case the grey band encompasses 95% of the considered sources.

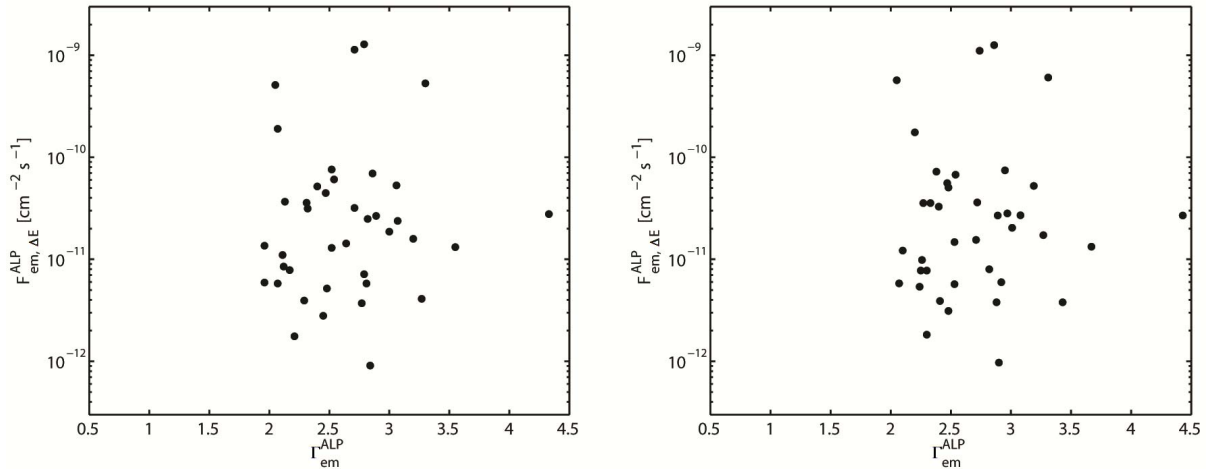


FIG. 9: *Left panel:* $F_{em,\Delta E}^{ALP}$ is plotted versus Γ_{em}^{ALP} for $\xi = 0.5$ and $L_{dom} = 4$ Mpc. *Right panel:* Same as left panel but for $\xi = 0.5$ and $L_{dom} = 10$ Mpc.

VI. DISCUSSION AND CONCLUSIONS

The main goal of the investigation reported in this paper concerns a possible correlation between the distribution of VHE blazar *emitted spectra* and the *redshift*.

Broadly speaking, two logically distinct results have been obtained, which can somewhat schematically be summarize as follows.

Working within conventional physics – and in particular within the two standard VHE photon emission models – we have shown that the emitted slope distribution $\{\Gamma_{em}^{CP}(z)\}$ exhibits a *correlation with z* , since the associated best-fit regression line is a *decreasing* function of z given by $\Gamma_{em}^{CP}(z) = 2.68 - 2.21z$, with $\chi_{red}^2 = 1.83$. This fact runs against physical intuition, since it is hard to understand how the source distribution can get to know the redshifts in such a way to adjust

their $\Gamma_{\text{em}}(z)$ values in such a way to reproduce such a statistical correlation. Indeed, this situation cannot be explained either by cosmological evolutionary effects or by observational selection biases. A further consequence is that blazars with harder spectra to be found *only* at larger redshift.

We have shown that a way out of this conundrum involves new physics in the form of ALPs, with photon-ALP oscillations taking place in the extragalactic magnetic field. Their result is ultimately to substantially reduce the level of EBL absorption. We have focussed our attention on two realistic benchmark cases: $L_{\text{dom}} = 4 \text{ Mpc}$ and $L_{\text{dom}} = 10 \text{ Mpc}$. After having worked out the effect of photon-ALP oscillations on the VHE emitted spectra starting from the observed ones, we have discovered that in either case the best-fit regression line pertaining to the $\{\Gamma_{\text{em}}^{\text{ALP}}(z)\}$ distribution turns out to be a straight line in the $\Gamma_{\text{em}}^{\text{ALP}} - z$ plane, hence *independent* of z . This circumstance looks astonishing. Of course, by changing the effective level of EBL absorption we obviously expect the z -dependence of the best-fit $\{\Gamma_{\text{em}}^{\text{ALP}}(z)\}$ distribution to differ from that of the $\{\Gamma_{\text{em}}^{\text{CP}}(z)\}$ distribution. As a consequence, the inclination of the best-fit straight regression line in the $\Gamma_{\text{em}} - z$ plane should change. But to become exactly horizontal – which is the only possibility in agreement with physical expectation – looks almost like a miracle. In addition, the values of $\Gamma_{\text{em}}^{\text{ALP}}(z)$ for the individual sources turn out to have a fairly small scatter about the considered best-fit straight regression line.

Actually, the considered ALP framework possesses further nice features.

- Even from a purely statistical point of view it is better than the conventional scenario, in which we have found $\chi_{\text{red}}^2 = 1.83$ for the best-fit straight regression line (Section III) or $\chi_{\text{red}}^2 = 2.35$ for the horizontal fitting straight line (Section IV). Instead now the best-fit straight regression lines in the right panels of Fig. 7 have $\chi_{\text{red}}^2 = 1.43$ for $L_{\text{dom}} = 4 \text{ Mpc}$ and $\chi_{\text{red}}^2 = 1.39$ for $L_{\text{dom}} = 10 \text{ Mpc}$. Note that this result has been obtained with a single free parameter.
- A new picture arises wherein a sharp distinction between *fundamental physics* and *boundary conditions* naturally emerges. The above discussion implies that 95% of the considered sources have a *small spread* in the values of $\Gamma_{\text{em}}^{\text{ALP}}(z)$. Specifically, $\Gamma_{\text{em}}^{\text{ALP}}(z)$ departs from the value of the best-fit straight regression line by *at most* 14% for $\xi = 0.5$ and $L_{\text{dom}} = 4 \text{ Mpc}$ and by 12% for $\xi = 0.5$ and $L_{\text{dom}} = 10 \text{ Mpc}$. Actually, the small scatter in the values of $\Gamma_{\text{em}}^{\text{ALP}}(z)$ implies that the emission mechanism is basically identical for all sources. On the other hand, the larger scatter in the values of $K_{\text{em}}(z)$ – presumably unaffected by photon-ALP oscillations when error bars are taken into account – is naturally traced back to the different environmental state of each source, such as for instance the accretion rate. A natural question should finally be addressed. How is it possible that the large scatter in $\{\Gamma_{\text{obs}}(z)\}$ distribution exhibited in the left panel of Fig. 1 arises from the small scatter in the $\{\Gamma_{\text{em}}^{\text{ALP}}(z)\}$ distribution shown in the left panels of Fig. 7? The answer is very simple: most of the scatter in the $\{\Gamma_{\text{obs}}(z)\}$ distribution arises from the large scatter in the source redshift.

Before closing this Section, we find it worthwhile to put the result of our investigation into its proper perspective.

During the last decade the interest in ALPs has been steadily growing. Various reasons have conspired towards this circumstance. With different motivations, the astrophysical implications of ALPs have been addressed since twenty years [36, 40–47]. Certainly the claimed discovery of an ALP by the PVLAS collaboration [48] in 2005, which – even if subsequently withdrawn by the PVLAS collaboration itself [49] – has provided a stimulus to look for astrophysical cross-checks [50–54]. Soon thereafter, it has been realized that several superstring theories predict the existence of

not only a single kind of ALP but more generally of a family of ALPs with very small masses [14–23]. As a matter of fact, the study of the relevance of ALPs for high-energy astrophysics has continued until the present [27, 55–92].

A tension between the predicted EBL level causing photon absorption and observations in the VHE range has been claimed from time to time (see e.g. [93, 94]), but then a better determination of the EBL properties has shown that no problem exists. As already stressed at the beginning of Section III, nowadays the situation is different, since different techniques basically lead to the same EBL model. Yet, it has recently been claimed that VHE observations require an EBL level even lower than that predicted by the minimal EBL model normalized to the galaxy counts only [95]. This is the so-called *pair-production anomaly*, which is based on the Kolmogorov test and so does not rely upon the estimated errors. It has thoroughly been quantified by a global statistical analysis of a large sample of observed blazars, showing that measurements in the regime of large optical depth deviate by 4.2σ from measurements in the optically thin regime [71]. Systematic effects have been shown to be insufficient to account for such the pair-production anomaly, which looks therefore real. Actually, the discovery of new blazars at large redshift like the observation of PKS 1424+240 have strengthened the case for the pair-production anomaly [83]. Quite recently, the existence of the pair-production anomaly has been questioned by using a new EBL model and a χ^2 test, in which errors play instead an important role [96]. Because the Kolmogorov test looks more robust in that it avoids taking errors into account, we tend to believe that the pair-production anomaly is indeed at the level of 4.2σ .

Amazingly, the existence of photon-ALP oscillations with the *same* realistic choice of the model parameters provides an excellent explanation for three *completely different* phenomena occurring in the VHE band.

- The pair-production anomaly is naturally explained in terms of photon-ALP oscillations in extragalactic magnetic fields [71, 79, 83]. This should hardly come as surprise, since – as already explained – the ultimate effect of photon-ALP oscillation is to substantially lower the effective EBL absorption level.
- According to conventional physics, flat spectrum radio quasars (FSRQs) should not emit above 20 – 30 GeV. This is due to the fact that higher energy photons accelerated in the jet enter – at a distance of about 1 kpc from the centre – the so-called broad-line region (BLR), whose high density of ultraviolet photons gives rise to an optical depth $\tau \simeq 15$ owing to the same $\gamma\gamma \rightarrow e^+e^-$ absorption process considered above. Even in this context, photon-ALP oscillations substantially lower the photon absorption level inside the BLR while still staying inside the standard blazar models, thereby allowing VHE photons to escape the BLR and be emitted, in remarkable quantitative agreement with observations [75]. We stress that the detection of VHE photons from FSRQs still represents a serious challenge for conventional models.
- Our findings described in the present paper show that the conventional scenario of photon propagation in extragalactic space is seriously challenged. Nevertheless, a physically satisfactory picture emerges by considering photon-ALP oscillations in the extragalactic magnetic field.

Altogether, such a situation evidently strongly suggests a preliminary evidence for the existence of an ALP, whose parameters make it a good candidate for cold dark matter [24]. Moreover, it looks tantalizing that the issue can definitively be settled not only with the advent of the new gamma-ray detectors like the CTA (Cherenkov Telescope Array) [97], HAWC (High-Altitude Water Cherenkov Observatory) [98], GAMMA-400 (Gamma Astronomical Multifunctional Modular Apparatus) [99],

LHAASO (Large High Altitude Air Shower Observatory) [100] and HiSCORE (Hundred Square km Cosmic Origin Explorer) [101], but also thanks to laboratory data based on the planned experiments ALPS II (Any Light Particle Search) [102, 103] and IAXO (International Axion Observatory) [104], which will have the capability to discover an ALP with the properties assumed in the present analysis. Also experiments exploiting the techniques discussed in [105–107] are quite promising for the laboratory detection of an ALP of this kind.

ACKNOWLEDGMENTS

We thank Patrizia Caraveo and Fabrizio Tavecchio for very useful discussions. We also thank Abelardo Moralejo, Andreas Ringwald and Sergey Troitsky for their comments. The work of M. R. is supported by INFN TAsP and CTA grants.

APPENDIX

Here we summarize the main properties of the ALP scenario considered in the text and the evaluation of the photon survival probability $P_{\gamma \rightarrow \gamma}^{\text{ALP}}(E_0, z)$.

A. General properties of axion-like particles (ALPs)

As already stated, ALPs are spin-zero, neutral and extremely light pseudo-scalar bosons similar to the *axion*, namely the pseudo-Goldstone boson associated with the global Peccei-Quinn symmetry $U(1)_{\text{PQ}}$ proposed as a natural solution to the strong CP problem [108]. The axion interacts with fermions, two gluons and two photons, and one of its characteristic feature is the existence of a strict linear relationship between its mass m and the two-photon coupling constant $g_{a\gamma\gamma}$

$$m = 0.7 k \left(g_{a\gamma\gamma} 10^{10} \text{ GeV} \right) \text{ eV} , \quad (13)$$

where k is a model-dependent constant of order 1 [109]. Nevertheless, ALPs differ from axions in two respects: (1) their mass m and two-photon coupling constant $g_{a\gamma\gamma}$ are *unrelated*, and (2) ALPs are supposed to interact *only* with two photons [13]. Hence, they are described by the Lagrangian

$$\mathcal{L}_{\text{ALP}} = \frac{1}{2} \partial^\mu a \partial_\mu a - \frac{1}{2} m^2 a^2 - \frac{1}{4} g_{a\gamma\gamma} F_{\mu\nu} \tilde{F}^{\mu\nu} a = \frac{1}{2} \partial^\mu a \partial_\mu a - \frac{1}{2} m^2 a^2 + g_{a\gamma\gamma} \mathbf{E} \cdot \mathbf{B} a , \quad (14)$$

where a and m are the ALP field and mass, respectively, and \mathbf{E} and \mathbf{B} are the electric and magnetic components of the field strength $F_{\mu\nu}$ ($\tilde{F}^{\mu\nu}$ is its dual).

We shall be concerned with the particular case of a monochromatic photon/ALP beam emitted by a blazar at redshift z and traveling through the ionized extragalactic space, where a magnetic field \mathbf{B} is supposed to exist with the domain-like structure described in Section VI. Therefore \mathbf{E} is the electric field of a beam photon while \mathbf{B} is the extragalactic magnetic field. In such a situation, the mass matrix of the photon-ALP system is non-diagonal, so that the propagation eigenstates differ from the interaction eigenstates. This fact gives rise to photon-ALP oscillations in the beam [110, 111], much in the same way as it happens in a beam of massive neutrinos of different flavor (however for photon-ALP oscillations an external magnetic field is needed to compensate for the spin mismatch). In order to avoid notational confusion, the symbol E will henceforth denote the energy of the beam particles.

Since we suppose that $E \gg m$ (more about this, later), we can employ the *short wavelength approximation*. As a consequence, the photon/ALP beam propagation turns out to be described by the following first-order Schrödinger-like equation with the time replaced by the y -coordinate along the beam [111]

$$\left(i \frac{d}{dy} + E + \mathcal{M} \right) \psi(y) = 0 \quad (15)$$

with wave function

$$\psi(y) \equiv \begin{pmatrix} A_x(y) \\ A_z(y) \\ a(y) \end{pmatrix} , \quad (16)$$

where $A_x(y)$ and $A_z(y)$ denote the photon amplitudes with polarization along the x - and z -axis, respectively, while $a(y)$ is the amplitude associated with the ALP. It is useful to introduce the 3-dimensional basis vectors $\{|\gamma_x\rangle, |\gamma_z\rangle, |a\rangle\}$ where $|\gamma_x\rangle \equiv (1, 0, 0)^T$ and $|\gamma_z\rangle \equiv (0, 1, 0)^T$ represent

the two photon linear polarization states along the x - and z -axis, respectively, and $|a\rangle \equiv (0, 0, 1)^T$ denotes the ALP state. Accordingly, we can write $\psi(y)$ as

$$\psi(y) = A_x(y) |\gamma_x\rangle + A_z(y) |\gamma_z\rangle + a(y) |a\rangle . \quad (17)$$

Note that the quantity $\mathcal{H} \equiv -(E + \mathcal{M})$ plays formally the role of the Hamiltonian. Denoting by $\mathcal{U}(y, y_0)$ the transfer matrix – namely the solution of Eq. (15) with initial condition $\mathcal{U}(y_0, y_0) = 1$ – the propagation of a generic wave function across the domain in question can be represented as

$$\psi(y) = \mathcal{U}(y, y_0) \psi(y_0) . \quad (18)$$

So far our attention has been restricted to the wave function, which describes a polarized beam. However, since in the gamma-ray band the polarization cannot be measured, we are forced to employ the density matrix $\rho(y)$. As in quantum mechanics, it obeys the analog of the Von Neumann equation associated with Eq. (15), whose form is

$$i \frac{d\rho}{dy} = \rho \mathcal{M}^\dagger - \mathcal{M} \rho . \quad (19)$$

As we shall see, EBL absorption implies that \mathcal{H} – and so \mathcal{M} and $\rho(y)$ – are not self-adjoint. Hence $\mathcal{U}(y, y_0)$ fails to be unitary. Nevertheless, it is trivial to check that the familiar relation

$$\rho(y) = \mathcal{U}(y, y_0) \rho(y_0) \mathcal{U}^\dagger(y, y_0) \quad (20)$$

retains its validity. Moreover, the probability that the beam in the state ρ_1 at y_0 will be found in the state ρ_2 at y is still given by the standard relation

$$P_{\rho_1 \rightarrow \rho_2}(y_0, y) = \text{Tr}(\rho_2 \mathcal{U}(y, y_0) \rho_1(y_0) \mathcal{U}^\dagger(y, y_0)) , \quad (21)$$

where it is supposed as usual that $\text{Tr} \rho_1 = \text{Tr} \rho_2 = 1$.

We stress that the advantage arising from the short wavelength approximation is that the beam propagation can *formally* be described as a three-level non-relativistic decaying quantum system.

It is quite enlightening to start by considering the beam propagation over a single magnetic domain and to neglect EBL absorption [57, 111] (this attitude indeed makes sense, since EBL absorption is independent of photon-ALP oscillations). Because then \mathbf{B} is homogeneous, we can choose the z -axis along \mathbf{B} so that $B_x = 0$. Correspondingly, the matrix \mathcal{M} entering Eq. (15) takes the form

$$\mathcal{M} = \begin{pmatrix} -\omega_{\text{pl}}^2/2E & 0 & 0 \\ 0 & -\omega_{\text{pl}}^2/2E & g_{a\gamma\gamma} B/2 \\ 0 & g_{a\gamma\gamma} B/2 & -m^2/2E \end{pmatrix} , \quad (22)$$

where ω_{pl} is the plasma frequency of the ionized intergalactic medium (IGM), which is related to the mean electron density n_e by $\omega_{\text{pl}} = 3.69 \cdot 10^{-11} (n_e/\text{cm}^{-3})^{1/2} \text{eV}$ [111]. So, by defining the oscillation wave number as

$$\Delta_{\text{osc}} \equiv \left[\left(\frac{m^2 - \omega_{\text{pl}}^2}{2E} \right)^2 + (g_{a\gamma\gamma} B)^2 \right]^{1/2} , \quad (23)$$

it is a simple exercise to show that the photon-ALP conversion probability across the considered domain is

$$P_{\gamma \rightarrow a}(L_{\text{dom}}) = \left(\frac{g_{a\gamma\gamma} B}{\Delta_{\text{osc}}} \right)^2 \sin^2 \left(\frac{\Delta_{\text{osc}} L_{\text{dom}}}{2} \right) . \quad (24)$$

Thus, defining the energy threshold [57]

$$E_L \equiv \frac{|m^2 - \omega_{\text{pl}}^2|}{2 g_{a\gamma\gamma} B} , \quad (25)$$

we see that in the *strong-mixing regime* – namely when condition $E > E_L$ is met – Eq. (23) reduces to

$$\Delta_{\text{osc}} \simeq g_{a\gamma\gamma} B \quad (26)$$

and consequently the photon-ALP conversion probability becomes maximal as well as *energy-independent*. Finally, since B and $g_{a\gamma\gamma}$ enter \mathcal{L}_{ALP} only in the combination $g_{a\gamma\gamma} B$, it proves instrumental to define the quantity

$$\xi \equiv \left(\frac{B}{\text{nG}} \right) (g_{a\gamma\gamma} 10^{11} \text{ GeV}) , \quad (27)$$

in terms of which Eq. (25) can be rewritten as

$$E_L \simeq \frac{25.64}{\xi} \left| \left(\frac{m}{10^{-10} \text{ eV}} \right)^2 - \left(\frac{\omega_{\text{pl}}}{10^{-10} \text{ eV}} \right)^2 \right| \text{ GeV} . \quad (28)$$

B. Model parameters

Before proceeding further, it is worthwhile to discuss the allowed values of the free parameters of the model. In this field, a signal is considered a discovery if its statistical significance is at least 5σ . Accordingly, the bounds should be divided into two classes, depending on whether their statistical significance is larger or smaller than 5σ .

- Those with statistical significance *larger* than 5σ prevent any discovery of an ALP, and to date only one bound belongs to this class: the one obtained by the CAST experiment at CERN, which reads $g_{a\gamma\gamma} < 8.8 \cdot 10^{-11} \text{ GeV}$ for $m < 0.02 \text{ eV}$ [112].
- All other weaker bounds provide useful information, but still allow for the discovery of an ALP. Various bounds of this sort have been derived, but we discuss here only those that we believe to be most relevant. One is based on the study of 39 Galactic globular clusters and slightly improves the CAST constraint giving $g_{a\gamma\gamma} < 6.6 \cdot 10^{-11} \text{ GeV}$ at the 2σ level (the mass range of its validity is not specified) [86]. Another has been obtained by the H.E.S.S. collaboration, looking at the source PKS 2155 – 304, from the absence of the characteristic fluctuating behavior of the realizations of the beam propagation around E_L (more about this, later) and reads $g_{a\gamma\gamma} < 2.1 \cdot 10^{-11} \text{ GeV}$ for $1.5 \cdot 10^{-8} \text{ eV} < m < 6.0 \cdot 10^{-8} \text{ eV}$ at the 2σ level [80]. A similar strategy has been applied to the source to the Hydra galaxy cluster, yielding $g_{a\gamma\gamma} < 8.3 \cdot 10^{-12} \text{ GeV}$ for $\text{eV} < m < 7.0 \cdot 10^{-12} \text{ eV}$ at the 2σ level [81]. Finally, the explosion of the 1987A supernova has been used to set an upper bound on $g_{a\gamma\gamma}$ depending on the value of m . The logic is as follows. Along with a neutrino burst lasting about 10 seconds, also an ALP burst should be emitted during the collapse. Inside the Galaxy magnetic field, some of the ALPs should convert into X-rays and next be detected by the Solar Maximal Mission (SMM) satellite. From the absence of detection, originally the bounds $g_{a\gamma\gamma} < 1.0 \cdot 10^{-11} \text{ GeV}$ for $m < 1.0 \cdot 10^{-9} \text{ eV}$ [41] and $g_{a\gamma\gamma} < 3.0 \cdot 10^{-12} \text{ GeV}$ for $m < 1.0 \cdot 10^{-9} \text{ eV}$ have been set [42]. A very recent analysis updating these two early works has been carried out, especially using the present state-of-the art knowledge of supernova

explosions (even if we still do not know why they actually explode). However, an unavoidable uncertainty affects the detection efficiency of the SMM, for instance the systematic error and the effective area, even because SN1987A was observed perpendicularly to the viewing direction of the SMM. The authors do not quote the statistical significance of this bound, which is certainly less than 2σ [92].

As far as the extragalactic magnetic field \mathbf{B} is concerned, the situation is much less clear-cut. A general consensus exists that it possesses a domain-like morphology (at least in first approximation) [37–39]. As mentioned in Section IV, it is supposed that \mathbf{B} is homogeneous over a domain of size L_{dom} equal to its coherence length, with \mathbf{B} *randomly* changing its direction from one domain to another but keeping approximately the same strength. Unfortunately, the values of both B and L_{dom} are largely unknown. We assume B to be pretty large according to the predictions of the galactic outflows models [25, 26]. Actually, within these models it looks natural to suppose that L_{dom} is of the order of the galactic correlation length, which amounts to take $L_{\text{dom}} = (1 - 10)$ Mpc in the present Universe ($z = 0$), even though larger values cannot be excluded. Then Fig. 4 of [113] implies that $B \leq 1$ nG, and so by taking the most restrictive bound on $g_{a\gamma\gamma}$ it follows from Eq. (27) that $\xi < 8$. The upper bound on the mean diffuse extragalactic electron density $n_e < 2.7 \cdot 10^{-7} \text{ cm}^{-3}$ is provided by the WMAP measurement of the baryon density [114], which – thanks to the above relation – translates into the upper bound $\omega_{\text{pl}} < 1.92 \cdot 10^{-14} \text{ eV}$. What about m ? In order to maximize the effect of photon-ALP oscillations we work throughout within the strong mixing regime. Recalling that the lower end of the VHE band is $E = 100 \text{ GeV}$, we then have to require $E_L < 100 \text{ GeV}$. Putting everything together and using Eq. (28) we find $m < 1.97 \cdot 10^{-10} \xi^{1/2}$, and at any rate we should have $m < 5 \cdot 10^{-10} \text{ eV}$. However, we remark that the size of the effect remains basically unchanged if the bound $E_L < 100 \text{ GeV}$ becomes less restrictive by a factor of a few, and so for all practical purposes we can assume $m < 10^{-9} \text{ eV}$. Finally, by combining the CAST bound $g_{a\gamma\gamma} < 8.8 \cdot 10^{-11} \text{ GeV}$ with the interaction term in \mathcal{L}_{ALP} , it is straightforward to get the following order-of-magnitude estimate for the cross-sections $\sigma(a\gamma \rightarrow f^+f^-) \sim \sigma(a f^\pm \rightarrow \gamma f^\pm) < 10^{-50} \text{ cm}^2$ (here f denotes any charged fermion), which show that effectively ALPs do not interact with anything and in particular with the EBL.

C. Strategy

One point should now be emphasized. Due to the nature of the extragalactic magnetic field, the angle of \mathbf{B} in each domain with a fixed fiducial direction equal for all domains (which we identify with the z -axis) is a random variable, and so the propagation of the photon/ALP beam becomes a N_d -dimensional *stochastic process*, where N_d denotes the total number of magnetic domains crossed by the beam. Therefore we identify the photon survival probability with its average value. Moreover, we shall see that the whole photon/ALP beam propagation can be recovered by iterating N_d times the propagation over a single magnetic domain, changing each time the value of the random angle. Thanks to the fact that \mathbf{B} is homogeneous in every domain, the beam propagation equation can be solved exactly in a single domain. Clearly, at the end we have to average the photon survival probability as evaluated for one arbitrary realization of the whole propagation process – namely for a particular choice of the random angle in each domain – over all possible realizations of the considered stochastic process (i.e. over all values of the random angle in each of the N_d domains) [115].

Our discussion is framed within the standard Λ CDM cosmological model with $\Omega_M = 0.3$ and $\Omega_\Lambda = 0.7$, and so the redshift is the natural parameter to express distances. In particular, the

proper length $L_{\text{dom}}(z_a, z_b)$ extending over the redshift interval $[z_a, z_b]$ is

$$L(z_a, z_b) \simeq 4.29 \cdot 10^3 \int_{z_a}^{z_b} \frac{dz}{(1+z)[0.7+0.3(1+z)^3]^{1/2}} \text{Mpc} \simeq 2.96 \cdot 10^3 \ln \left(\frac{1+1.45 z_b}{1+1.45 z_a} \right) \text{Mpc}. \quad (29)$$

Accordingly, the overall structure of the cellular configuration of the extragalactic magnetic field is naturally described by a *uniform* mesh in redshift space with elementary step Δz , which is therefore the same for all domains. This mesh can be constructed as follows. We denote by $L_{\text{dom}}^{(n)} = L((n-1)\Delta z, n\Delta z)$ the proper length along the y -direction of the generic n -th domain, with $1 \leq n \leq N_d$, where the total number of magnetic domains N_d towards the considered blazar is the maximal integer contained in the number $z/\Delta z$, hence $N_d \simeq z/\Delta z$. In order to fix Δz we consider the domain closest to us, labelled by 1 and – with the help of Eq. (29) – we write its proper length as $(L_{\text{dom}}^{(1)}/5 \text{Mpc}) 5 \text{Mpc} = L(0, \Delta z) = 2.96 \cdot 10^3 \ln(1+1.45 \Delta z) \text{Mpc}$, from which we get $\Delta z \simeq 1.17 \cdot 10^{-3} (L_{\text{dom}}^{(1)}/5 \text{Mpc})$. So, once $L_{\text{dom}}^{(1)}$ is chosen in agreement with the previous considerations, the size of *all* magnetic domains in redshift space is fixed. At this point, two further quantities can be determined. First, the total number of the considered domains is $N_d \simeq z/\Delta z \simeq 0.85 \cdot 10^3 (5 \text{Mpc}/L_{\text{dom}}^{(1)}) z$. Second, the proper length of the n -th domain along the y -direction follows from Eq. (29) with $z_a \rightarrow (n-1)\Delta z, z_b \rightarrow n\Delta z$. Whence

$$L_{\text{dom}}^{(n)} \simeq 2.96 \cdot 10^3 \ln \left(1 + \frac{1.45 \Delta z}{1+1.45(n-1)\Delta z} \right) \text{Mpc}. \quad (30)$$

D. Propagation over a single domain

What still has to be done is to take EBL absorption into account and to determine the magnetic field strength $B^{(n)}$ in the generic n -th domain.

The first goal can be achieved by simply following the discussion of [115]. Because the domain size is so small as compared to the cosmological standards, we can safely drop cosmological evolutionary effects when considering a single domain. Then as far as absorption is concerned what matters is the mean free path λ_γ for the reaction $\gamma\gamma \rightarrow e^+e^-$, and the term $i/2\lambda_\gamma$ should be inserted into the 11 and 22 entries of the \mathcal{M} matrix. In order to evaluate λ_γ , we imagine that two hypothetical sources located at both edges of the n -th domain are observed. Therefore, we insert Eq. (2) into Eq. (1) of Section I and further apply the resulting equation to both of them. With the notational simplifications $\Phi_{\text{obs}}(E_0, z) \rightarrow \Phi(E_0)$ and $\Phi_{\text{em}}(E_0(1+z)) \rightarrow \Phi(E_0(1+z))$, we have

$$\Phi(E_0) = e^{-\tau_\gamma(E_0, (n-1)\Delta z)} \Phi(E_0[1+(n-1)\Delta z]), \quad \Phi(E_0) = e^{-\tau_\gamma(E_0, n\Delta z)} \Phi(E_0(1+n\Delta z)), \quad (31)$$

which upon combination imply that the flux change across the domain in question is

$$\Phi(E_0[1+(n-1)\Delta z]) = e^{-[\tau_\gamma(E_0, n\Delta z) - \tau_\gamma(E_0, (n-1)\Delta z)]} \Phi(E_0(1+n\Delta z)). \quad (32)$$

Because cosmological effects can be neglected across a single domain, Eq. (32) should have the usual form

$$\Phi(E_0[1+(n-1)\Delta z]) = e^{-L_{\text{dom}}^{(n)}/\lambda_\gamma^{(n)}(E_0)} \Phi(E_0, (1+n\Delta z)), \quad (33)$$

and the comparison with Eq. (32) ultimately yields

$$\lambda_\gamma^{(n)}(E_0) = \frac{L_{\text{dom}}^{(n)}}{\tau_\gamma(E_0, n\Delta z) - \tau_\gamma(E_0, (n-1)\Delta z)}, \quad (34)$$

where the optical depth is evaluated as stated in the text for the EBL model of FRV [29].

To accomplish the second task, we note that because of the high conductivity of the IGM medium the magnetic flux lines can be thought as frozen inside it [39]. Therefore the flux conservation during the cosmic expansion entails that B scales like $(1+z)^2$, so that the magnetic field strength in a domain at redshift z is $B(z) = B(z=0)(1+z)^2$. Hence in the n -th magnetic domain we have $B^{(n)} = B^{(1)}(1+(n-1)\Delta z)^2$.

So, at this stage the matrix \mathcal{M} in Eq. (15) as explicitly written in the n -th domain reads

$$\mathcal{M}^{(n)} = \begin{pmatrix} i/2\lambda_\gamma^{(n)} & 0 & B^{(n)} \sin \psi_n g_{a\gamma\gamma}/2 \\ 0 & i/2\lambda_\gamma^{(n)} & B^{(n)} \cos \psi_n g_{a\gamma\gamma}/2 \\ B^{(n)} \sin \psi_n g_{a\gamma\gamma}/2 & B^{(n)} \cos \psi_n g_{a\gamma\gamma}/2 & 0 \end{pmatrix}, \quad (35)$$

where ψ_n is the random angle between $\mathbf{B}^{(n)}$ and the fixed fiducial direction along the z -axis (note that indeed $\mathcal{M}^\dagger \neq \mathcal{M}$). Apart from ψ_n , all other matrix elements entering $\mathcal{M}^{(n)}$ are known. Finding the transfer matrix of Eq. (15) with $\mathcal{M}^{(n)}$ given by Eq. (35) is a straightforward even if somewhat boring game. The result is

$$\mathcal{U}_n(E_n, \psi_n) = e^{iE_n L_{\text{dom}}^{(n)}} \left[e^{i(\lambda_1^{(n)} L_{\text{dom}}^{(n)})} T_1(\psi_n) + e^{i(\lambda_2^{(n)} L_{\text{dom}}^{(n)})} T_2(\psi_n) + e^{i(\lambda_3^{(n)} L_{\text{dom}}^{(n)})} T_3(\psi_n) \right] \quad (36)$$

with

$$T_1(\psi_n) \equiv \begin{pmatrix} \cos^2 \psi_n & -\sin \psi_n \cos \psi_n & 0 \\ -\sin \psi_n \cos \psi_n & \sin^2 \psi_n & 0 \\ 0 & 0 & 0 \end{pmatrix}, \quad (37)$$

$$T_2(\psi_n) \equiv \begin{pmatrix} \frac{-1+\sqrt{1-4\delta_n^2}}{2\sqrt{1-4\delta_n^2}} \sin^2 \psi_n & \frac{-1+\sqrt{1-4\delta_n^2}}{2\sqrt{1-4\delta_n^2}} \sin \psi_n \cos \psi_n & \frac{i\delta_n}{\sqrt{1-4\delta_n^2}} \sin \psi_n \\ \frac{-1+\sqrt{1-4\delta_n^2}}{2\sqrt{1-4\delta_n^2}} \sin \psi_n \cos \psi_n & \frac{-1+\sqrt{1-4\delta_n^2}}{2\sqrt{1-4\delta_n^2}} \cos^2 \psi_n & \frac{i\delta_n}{\sqrt{1-4\delta_n^2}} \cos \psi_n \\ \frac{i\delta_n}{\sqrt{1-4\delta_n^2}} \sin \psi_n & \frac{i\delta_n}{\sqrt{1-4\delta_n^2}} \cos \psi_n & \frac{1+\sqrt{1-4\delta_n^2}}{2\sqrt{1-4\delta_n^2}} \end{pmatrix}, \quad (38)$$

$$T_3(\psi_n) \equiv \begin{pmatrix} \frac{1+\sqrt{1-4\delta_n^2}}{2\sqrt{1-4\delta_n^2}} \sin^2 \psi_n & \frac{1+\sqrt{1-4\delta_n^2}}{2\sqrt{1-4\delta_n^2}} \sin \psi_n \cos \psi_n & \frac{-i\delta_n}{\sqrt{1-4\delta_n^2}} \sin \psi_n \\ \frac{1+\sqrt{1-4\delta_n^2}}{2\sqrt{1-4\delta_n^2}} \sin \psi_n \cos \psi_n & \frac{1+\sqrt{1-4\delta_n^2}}{2\sqrt{1-4\delta_n^2}} \cos^2 \psi_n & \frac{-i\delta_n}{\sqrt{1-4\delta_n^2}} \cos \psi_n \\ \frac{-i\delta_n}{\sqrt{1-4\delta_n^2}} \sin \psi_n & \frac{-i\delta_n}{\sqrt{1-4\delta_n^2}} \cos \psi_n & \frac{-1+\sqrt{1-4\delta_n^2}}{2\sqrt{1-4\delta_n^2}} \end{pmatrix}, \quad (39)$$

where we have set

$$\lambda_1^{(n)} \equiv \frac{i}{2\lambda_\gamma^{(n)}(E_0)}, \quad \lambda_2^{(n)} \equiv \frac{i}{4\lambda_\gamma^{(n)}} \left(1 - \sqrt{1-4\delta_n^2}\right), \quad \lambda_3^{(n)} \equiv \frac{i}{4\lambda_\gamma^{(n)}} \left(1 + \sqrt{1-4\delta_n^2}\right) \quad (40)$$

with

$$E_n \equiv E_0 \left[1 + (n-1)\Delta z\right], \quad \delta_n \equiv \xi_n \lambda_\gamma^{(n)}(E_0) \left(\frac{\text{nG}}{10^{11} \text{ GeV}}\right), \quad (41)$$

where ξ_n is just ξ as defined by Eq. (27) and evaluated in the n -th domain.

E. Calculation of the photon survival probability in the presence of photon-ALP oscillations

Our aim is to derive the photon survival probability $P_{\gamma\gamma}^{\text{ALP}}(E_0, z)$ entering the text. So far, we have dealt with a single magnetic domain but now we enlarge our view so as to encompass the whole propagation process of the beam from the source to us. This goal is trivially achieved thanks to the analogy with non-relativistic quantum mechanics, according to which – for a fixed arbitrary choice of the angles $\{\psi_n\}_{1 \leq n \leq N_d}$ – the whole transfer matrix describing the propagation of the photon/ALP beam from the source at redshift z to us is

$$\mathcal{U}(E_0, z; \psi_1, \dots, \psi_{N_d}) = \prod_{n=1}^{N_d} \mathcal{U}_n(E_n, \psi_n) . \quad (42)$$

Moreover, the probability that a photon/ALP beam emitted by a blazar at z in the state ρ_1 will be detected in the state ρ_2 for the above choice of $\{\psi_n\}_{1 \leq n \leq N_d}$ is given by Eq. (21). Whence

$$P_{\rho_1 \rightarrow \rho_2}(E_0, z; \psi_1, \dots, \psi_{N_d}) = \text{Tr} \left(\rho_2 \mathcal{U}(E_0, z; \psi_1, \dots, \psi_{N_d}) \rho_1 \mathcal{U}^\dagger(E_0, z; \psi_1, \dots, \psi_{N_d}) \right) \quad (43)$$

with $\text{Tr} \rho_1 = \text{Tr} \rho_2 = 1$.

Since the actual values of the angles $\{\psi_n\}_{1 \leq n \leq N_d}$ are unknown, the best that we can do is to evaluate the probability entering Eq. (43) as averaged over all possible values of the considered angles, namely

$$P_{\rho_1 \rightarrow \rho_2}(E_0, z) = \left\langle P_{\rho_1 \rightarrow \rho_2}(E_0, z; \psi_1, \dots, \psi_{N_d}) \right\rangle_{\psi_1, \dots, \psi_{N_d}} , \quad (44)$$

indeed in accordance with the strategy outlined above. In practice, this is accomplished by evaluating the r.h.s. of Eq. (43) over a very large number of realizations of the propagation process (we take 5000 realizations) randomly choosing the values of all angles $\{\psi_n\}_{1 \leq n \leq N_d}$ for every realization, adding the results and dividing by the number of realizations.

Because the photon polarization cannot be measured at the considered energies, we have to sum the result over the two final polarization states

$$\rho_x = \begin{pmatrix} 1 & 0 & 0 \\ 0 & 0 & 0 \\ 0 & 0 & 0 \end{pmatrix} , \quad (45)$$

$$\rho_z = \begin{pmatrix} 0 & 0 & 0 \\ 0 & 1 & 0 \\ 0 & 0 & 0 \end{pmatrix} . \quad (46)$$

Moreover, we suppose here that the emitted beam consists 100% of unpolarized photons, so that the initial beam state is described by the density matrix

$$\rho_{\text{unpol}} = \frac{1}{2} \begin{pmatrix} 1 & 0 & 0 \\ 0 & 1 & 0 \\ 0 & 0 & 0 \end{pmatrix} . \quad (47)$$

We find in this way the photon survival probability $P_{\gamma\gamma}^{\text{ALP}}(E_0, z)$

$$\begin{aligned} P_{\gamma\gamma}^{\text{ALP}}(E_0, z) &= \left\langle P_{\rho_{\text{unpol}} \rightarrow \rho_x}(E_0, z; \psi_1, \dots, \psi_{N_d}) \right\rangle_{\psi_1, \dots, \psi_{N_d}} + \\ &+ \left\langle P_{\rho_{\text{unpol}} \rightarrow \rho_z}(E_0, z; \psi_1, \dots, \psi_{N_d}) \right\rangle_{\psi_1, \dots, \psi_{N_d}} , \end{aligned} \quad (48)$$

which is indeed the quantity entering Eq. (11) of the text.

A final remark is in order. It is obvious that the beam follows a single realization of the considered stochastic process at once, but since we do not know which one is actually selected the best we can do is to evaluate the average photon survival probability. Nevertheless, it can be shown that the considered realizations exhibit an oscillatory behavior for an energy close to the threshold E_L defined by Eq. (25). Therefore, observations performed at energies close enough to E_L should exhibit oscillations in the energy spectrum [73, 82]. This fact has been used to derive the previous bounds discussed in [80, 81].

-
- [1] <https://www.mpi-hd.mpg.de/hfm/HESS>
- [2] <https://magic.mpp.mpg.de/>
- [3] <http://veritas.sao.arizona.edu/>
- [4] <http://tevcat.uchicago.edu/>
- [5] E. Dwek, F. Krennrich, *Astroparticle Phys.* **43**, 112 (2013).
- [6] S. D. Bloom, A. P. Marscher, *Astrophys. J.* **461**, 657 (1996).
- [7] F. Tavecchio, L. Maraschi, G. Ghisellini, *Astrophys. J.* **509**, 608 (1998).
- [8] F. A. Aharonian, *Very High Energy Cosmic Gamma Radiation* (World Scientific, Singapore, 2004).
- [9] W. Essey and A. Kusenko, *Astroparticle Physics* **33**, 81 (2010).
- [10] A. Prosekin, W. Essey, A. Kusenko and F. Aharonian, *Astrophys. J.* **757**, 183 (2012).
- [11] K. Murase, C. D. Dermer, H. Takami and G. Migliori, *Astrophys. J.* **749**, 63 (2012).
- [12] G. Bonnoli, F. Tavecchio, G. Ghisellini and T. Sbarrato, arXiv:1501.01974.
- [13] J. Jaeckel and A. Ringwald, *Ann. Rev. Nucl. Part. Sci.* **60**, 405 (2010).
- [14] N. Turok, *Phys. Rev. Lett.* **76**, 1015 (1996).
- [15] E. Witten, *Phys. Lett. B* **149**, 351 (1984).
- [16] J. P. Conlon, *JHEP* **0605**, 078 (2006).
- [17] P. Svrcek and E. Witten, *JHEP* **0606**, 051 (2006).
- [18] J. P. Conlon, *Phys. Rev. Lett.* **97**, 261802 (2006).
- [19] K. -S. Choi, I. -W. Kim and J. E. Kim, *JHEP* **0703**, 116 (2007).
- [20] A. Arvanitaki et al., *Phys. Rev. D* **81**, 123530 (2010).
- [21] B. S. Acharya, K. Bobkov and P. Kumar, *JHEP* **1011**, 105 (2010).
- [22] M. Cicoli, M. Goodsell and A. Ringwald, *JHEP* **1210**, 146 (2012).
- [23] A. G. Dias, A. C. B. Machado, C. C. Nishi, A. Ringwald and P. Vaudrevange, *JHEP* **1406**, 037 (2014).
- [24] P. Arias *et al.*, *JCAP* **06**, 008 (2012).
- [25] S. R. Furlanetto and A. Loeb, *Astrophys. J.* **556**, 619 (2001).
- [26] S. Bertone, C. Vogt and T. Ensslin, *Mon. Not. R. Astron. Soc.* **370**, 319 (2006).
- [27] A. De Angelis, M. Roncadelli, O. Mansutti, *Phys. Rev. D* **76**, 121301 (2007).
- [28] A. De Angelis, G. Galanti and M. Roncadelli, *Mon. Not. R. Astron. Soc.* **432**, 3245 (2013).
- [29] A. Franceschini, G. Rodighiero, E. Vaccari, *Astron. Astrophys.* **487**, 837 (2008).
- [30] G. Breit, J. A. Wheeler, *Phys. Rev.* **46**, 1087 (1934).
- [31] W. Heitler, *The Quantum Theory of Radiation* (Oxford University Press, Oxford, 1960).
- [32] A. I. Nikishov, *Sov. Phys. JETP* **14**, 393 (1962).
- [33] R. J. Gould, G. P. Schröder, *Phys. Rev.* **155**, 1407 (1967).
- [34] G. G. Fazio, F. W. Stecker, *Nature* **226**, 135 (1970).
- [35] F. Tavecchio *et al.*, *Mon. Not. R. Astron. Soc.* **401**, 1570 (2010).
- [36] Y. Grossman, S. Roy and J. Zupan, *Phys. Lett. B* **543**, 23 (2002).
- [37] P. P. Kronberg, *Rept. Prog. Phys.* **57**, 325 (1994).
- [38] P. Blasi, S. Bures and A. V. Olinto, *Astrophys. J.* **514**, L79 (1999).
- [39] D. Grasso and H. R. Rubinstein, *Phys. Rep.* **348**, 163 (2001).
- [40] E. Massó and R. Toldra, *Phys. Rev. D* **52**, 1755 (1995).
- [41] J. W. Brockway, E. D. Carlson, G. G. Raffelt, *Phys. Lett. B* **383**, 439 (1996).
- [42] J. A. Grifols, E. Massó and R. Toldrá, *Phys. Rev. Lett.* **77**, 2372 (1996).
- [43] E. Massó and R. Toldra, *Phys. Rev. D* **55**, 7967 (1997).
- [44] S. M. Carroll, *Phys. Rev. Lett.* **81**, 3067 (1998).
- [45] C. Csáki, N. Kaloper and J. Terning, *Phys. Rev. Lett.* **88**, 161302 (2002).
- [46] C. Csáki, N. Kaloper and J. Terning, *Phys. Lett. B* **535**, 33 (2002).
- [47] M. Christensson and M. Fairbairn, *Phys. Lett. B* **565**, 10 (2003).
- [48] E. Zavattini *et al.*, *Phys. Rev. Lett.* **96**, 110406 (2006).
- [49] E. Zavattini *et al.*, *Phys. Rev. Lett.* **99**, 129901 (2007).
- [50] A. Dupays, C. Rizzo, M. Roncadelli and G. F. Bignami, *Phys. Rev. Lett.* **95**, 211302 (2005).
- [51] E. Massó and J. Redondo, *JCAP* **05**, 015 (2005).
- [52] C. Corianó and N. Irges, *Phys. Lett. B* **651**, 298 (2007).
- [53] M. Fairbairn, T. Rashba and S. Troitsky, *Phys. Rev. Lett.* **98**, 201801 (2007).

- [54] A. Mirizzi, G. G. Raffelt and P. D. Serpico, Phys. Rev. D **76**, 023001 (2007).
- [55] D. Hooper and P. D. Serpico, Phys. Rev. Lett. **99**, 231102 (2007).
- [56] K. A. Hochmuth and G. Sigl, Phys. Rev. D **76**, 123011 (2007).
- [57] A. De Angelis, O. Mansutti and M. Roncadelli, Phys. Lett. B **659**, 847 (2008).
- [58] M. Simet, D. Hooper and P. D. Serpico, Phys. Rev. D **77**, 063001 (2008).
- [59] A. De Angelis, O. Mansutti, M. Persic and M. Roncadelli, Mon. Not. R. Astron. Soc. **394**, L21 (2009).
- [60] A. Mirizzi and D. Montanino, JCAP **12**, 004 (2009).
- [61] D. Chelouche, R. Rabadan, S. S. Pavlov and F. Castejon, Astrophys. J. Suppl. **180**, 1 (2009).
- [62] D. Chelouche and E. Guendelman, Astrophys. J. **699**, L5 (2009).
- [63] C. Burrage, A.-C. Davis and D. J. Shaw, Phys. Rev. D **79**, 044028 (2009).
- [64] M. A. Sánchez-Conde *et al.*, Phys. Rev. D **79**, 123511 (2009).
- [65] N. Bassan, A. Mirizzi and M. Roncadelli, JCAP **05**, 010 (2010).
- [66] O. Mena, S. Razzaque and F. Villaescusa-Navarro, JCAP **02**, 030 (2011).
- [67] A. Domínguez, M. A. Sánchez-Conde and F. Prada, JCAP **11**, 020 (2011).
- [68] R. Gill and J. S. Heyl, Phys. Rev. D **84**, 085001 (2011).
- [69] A. Payez, J. R. Cudell and D. Hutsemekers, Phys. Rev. D **84**, 085029 (2011).
- [70] M. Fairbairn, T. Rashba and S. Troitsky, Phys. Rev. D **84**, 125019 (2011).
- [71] D. Horns and M. Meyer, JCAP **02**, 033 (2012).
- [72] D. Horns, L. Maccione, A. Mirizzi and M. Roncadelli, Phys. Rev. D **85**, 085021 (2012).
- [73] D. Wouters, P. Brun, Phys. Rev. D **86**, 043005 (2012).
- [74] D. Horns *et al.*, Phys. Rev. D **86**, 075024 (2012).
- [75] F. Tavecchio, M. Roncadelli, G. Galanti and G. Bonnoli, Phys. Rev. D **86**, 085036 (2012).
- [76] A. Friedland, M. Giannotti and M. Wise, Phys. Rev. Lett. **110**, 061101 (2013).
- [77] G. Carosi *et al.*, A snowmass white paper, arXiv:1309.7035.
- [78] J. P. Conlon and M. C. D. Marsh, Phys. Rev. Lett. **111**, 151301 (2013).
- [79] M. Meyer, D. Horns and M. Raue, Phys. Rev. D **87**, 035027 (2013).
- [80] A. Abramowski *et al.* [HESS Collaboration], Phys. Rev. D **88**, 102003 (2013).
- [81] D. Wouters and P. Brun, Astrophys. J. **772**, 44 (2013).
- [82] G. Galanti, M. Roncadelli, arXiv:1305.2114.
- [83] M. Meyer and D. Horns, arXiv:1310.2058.
- [84] M. Meyer, D. Montanino and J. Conrad, JCAP **09**, 003 (2014).
- [85] S. Angus, J. P. Conlon, M. C. D. Marsh, A. Powell and L. T. Witkowski, JCAP **09**, 026 (2014).
- [86] A. Ayala *et al.*, Phys. Rev. Lett. **113**, 191302 (2014).
- [87] G. I. Rubtsov and S. V. Troitsky, JETP Lett. **100**, 355 (2014).
- [88] F. Tavecchio, G. Galanti and M. Roncadelli, arXiv:1406.2303.
- [89] D. Wouters and P. Brun, JCAP **01**, 016 (2014).
- [90] J. Harris, P. M. Chadwick, JCAP **10**, 018 (2014).
- [91] M. Meyer and J. Conrad, JCAP **12**, 016 (2014).
- [92] A. Payez *et al.*, arXiv:1410.3747.
- [93] R. J. Protheroe and H. Meyer, Phys. Lett. B **493**, 1 (2000).
- [94] F. T. Aharonian *et al.* [H.E.S.S. Collaboration], Nature **440**, 1018 (2006).
- [95] T. M. Kneiske and H. Dole, Astron. Astrophys. **515**, 19 (2010).
- [96] J. Biteau and D. A. Williams, arXiv:1502.04166.
- [97] <https://www.cta-observatory.org/>.
- [98] www.hawc-observatory.org/
- [99] gamma400.lebedev.ru/gamma400_e.html
- [100] <http://english.ihep.cas.cn/ic/ip/LHAASO/>
- [101] www.desy.de/groups/astroparticle/score/en/
- [102] <https://alps.desy.de/e141064>.
- [103] R. Bähre *et al.*, arXiv:1302.5647.
- [104] I. G. Irastorza *et al.* [IAEXO Collaboration], JCAP **06**, 013 (2011).
- [105] F. T. Avignone III, Phys. Rev. D **79**, 035015 (2009).
- [106] F. T. Avignone III, R. J. Crewick and S. Nussinov, Phys. Lett. B **681**, 122 (2009).
- [107] F. T. Avignone III, R. J. Crewick and S. Nussinov, Astropart. Phys. **34**, 640 (2011).
- [108] For a review, see: J. E. Kim and G. Carosi, Rev. Mod. Phys. **82**, 557 (2010).

- [109] S. L. Cheng, C. Q. Geng, and W. T. Ni, *Phys. Rev. D* **52**, 3132 (1995).
- [110] P. Sikivie, *Phys. Rev. Lett.* **51**, 1415 (1983); (E) *Phys. Rev. Lett.* **52**, 695 (1984).
- [111] G. G. Raffelt, L. Stodolsky, *Phys. Rev. D* **37**, 1237 (1988).
- [112] E. Arik *et al.* [CAST collaboration], *JCAP* **02**, 008 (2009).
- [113] R. Durrer and A. Neronov, *Astron. Astrophys. Rev.* **21**, 62 (2013).
- [114] G. Hinshaw *et al.* [WMAP collaboration], *Astrophys. J. Suppl.* **180**, 225 (2009).
- [115] C. Csáki, N. Kaloper, M. Peloso, J. Terning, *JCAP* **05**, 005 (2003).

Source	z	Γ_{obs}	ΔE_0 [TeV]	K_{obs} [$\text{cm}^{-2} \text{s}^{-1} \text{TeV}^{-1}$]
3C 66B	0.0215	3.10 ± 0.37	0.12 – 1.8	$1.74 \cdot 10^{-11}$
Mrk 421	0.031	2.20 ± 0.22	0.13 – 2.7	$6.43 \cdot 10^{-10}$
Mrk 501	0.034	2.72 ± 0.18	0.21 – 2.5	$1.53 \cdot 10^{-10}$
1ES 2344+514	0.044	2.95 ± 0.23	0.17 – 4.0	$5.42 \cdot 10^{-11}$
Mrk 180	0.045	3.30 ± 0.73	0.18 – 1.3	$4.50 \cdot 10^{-11}$
1ES 1959+650	0.048	2.72 ± 0.24	0.19 – 1.5	$8.99 \cdot 10^{-11}$
1ES 1959+650	0.048	2.58 ± 0.27	0.19 – 2.4	$6.03 \cdot 10^{-11}$
AP LIB	0.049	2.50 ± 0.22	0.30 – 3.0	?
1ES 1727+502	0.055	2.70 ± 0.54	0.10 – 0.6	$9.60 \cdot 10^{-12}$
PKS 0548-322	0.069	2.86 ± 0.35	0.32 – 3.5	$1.10 \cdot 10^{-11}$
BL Lacertae	0.069	3.60 ± 0.43	0.15 – 0.7	$5.80 \cdot 10^{-10}$
PKS 2005-489	0.071	3.20 ± 0.19	0.32 – 3.3	$3.44 \cdot 10^{-11}$
RGB J0152+017	0.08	2.95 ± 0.41	0.32 – 3.0	$1.99 \cdot 10^{-11}$
1ES 1741+196	0.083	?	?	?
SHBL J001355.9-185406	0.095	3.40 ± 0.54	0.42 – 2.0	$7.05 \cdot 10^{-12}$
W Comae	0.102	3.81 ± 0.49	0.27 – 1.1	$5.98 \cdot 10^{-11}$
1ES 1312-423	0.105	2.85 ± 0.51	0.36 – 4.0	$5.85 \cdot 10^{-12}$
VER J0521+211	0.108	3.44 ± 0.36	0.22 – 1.1	$5.35 \cdot 10^{-11}$
PKS 2155-304	0.116	3.53 ± 0.12	0.21 – 4.1	$1.27 \cdot 10^{-10}$
B3 2247+381	0.1187	3.20 ± 0.71	0.15 – 0.84	$1.40 \cdot 10^{-11}$
RGB J0710+591	0.125	2.69 ± 0.33	0.37 – 3.4	$1.49 \cdot 10^{-11}$
H 1426+428	0.129	3.55 ± 0.49	0.28 – 0.43	$1.46 \cdot 10^{-10}$
1ES 1215+303	0.13	3.60 ± 0.50	0.30 – 0.85	$2.30 \cdot 10^{-11}$
1ES 1215+303	0.13	2.96 ± 0.21	0.095 – 1.3	$2.27 \cdot 10^{-11}$
RX J1136.5+6737	0.1342	?	?	?
1ES 0806+524	0.138	3.60 ± 1.04	0.32 – 0.63	$1.92 \cdot 10^{-11}$
1ES 0229+200	0.14	2.50 ± 0.21	0.58 – 11	$1.12 \cdot 10^{-11}$
1RXS J101015.9-311909	0.142639	3.08 ± 0.47	0.26 – 2.2	$7.63 \cdot 10^{-12}$
H 2356-309	0.165	3.09 ± 0.26	0.22 – 0.9	$1.24 \cdot 10^{-11}$
RX J0648.7+1516	0.179	4.40 ± 0.85	0.21 – 0.47	$2.30 \cdot 10^{-11}$
1ES 1218+304	0.182	3.08 ± 0.39	0.18 – 1.4	$3.62 \cdot 10^{-11}$
1ES 1101-232	0.186	2.94 ± 0.22	0.28 – 3.2	$1.94 \cdot 10^{-11}$
1ES 0347-121	0.188	3.10 ± 0.25	0.30 – 3.0	$1.89 \cdot 10^{-11}$
RBS 0413	0.19	3.18 ± 0.74	0.30 – 0.85	$1.38 \cdot 10^{-11}$
RBS 0723	0.198	?	?	?
1ES 1011+496	0.212	4.00 ± 0.54	0.16 – 0.6	$3.95 \cdot 10^{-11}$
MS 1221.8+2452	0.218	?	?	?
PKS 0301-243	0.2657	4.60 ± 0.73	0.25 – 0.52	$8.56 \cdot 10^{-12}$
1ES 0414+009	0.287	3.45 ± 0.32	0.18 – 1.1	$6.03 \cdot 10^{-12}$
S5 0716+714	0.31	3.45 ± 0.58	0.18 – 0.68	$1.40 \cdot 10^{-10}$
1ES 0502+675	0.341	3.92 ± 0.36	?	?
PKS 1510-089	0.361	5.40 ± 0.76	0.14 – 0.32	$6.97 \cdot 10^{-12}$
3C 66A	0.41	4.10 ± 0.72	0.23 – 0.47	$4.00 \cdot 10^{-11}$
PKS 1222+216	0.432	3.75 ± 0.34	0.08 – 0.36	$1.71 \cdot 10^{-10}$
1ES 0647+250	0.45	?	?	?
PG 1553+113	0.5	4.50 ± 0.32	0.23 – 1.1	$4.68 \cdot 10^{-11}$
3C 279	0.5362	4.10 ± 0.73	0.08 – 0.46	$9.86 \cdot 10^{-11}$
PKS 1424+240	≥ 0.6035	3.80 ± 0.58	0.14 – 0.5	$1.09 \cdot 10^{-11}$

TABLE III: Considered VHE blazars with known energy, redshift, spectral slope Γ_{obs} , energy range and normalization constant K_{obs} . Statistical and systematic errors are added in quadrature to produce the total error reported on the measured spectral slope. When only statistical errors are quoted, systematic errors are taken to be 0.1 for H.E.S.S., 0.15 for VERITAS, and 0.2 for MAGIC. Sources with question marks lack information to perform our analysis and are discarded. For PKS 1424+240 only a lower limit on the redshift exists in the literature: thus, it is neglected in our analysis.

Source	$\Gamma_{\text{em}}^{\text{CP}}$	$\Gamma_{\text{em}}^{\text{ALP}}$			
		$\xi = 0.1$	$\xi = 0.5$	$\xi = 1$	$\xi = 5$
3C 66B	3.00	3.00	3.00	3.01	3.03
Mrk 421	2.05	2.05	2.05	2.06	2.10
Mrk 501	2.54	2.54	2.54	2.55	2.59
1ES 2344+514	2.71	2.71	2.71	2.73	2.79
Mrk 180	3.07	3.07	3.07	3.09	3.14
1ES 1959+650	2.46	2.46	2.47	2.49	2.55
1ES 1959+650	2.32	2.32	2.32	2.35	2.40
AP LIB	2.21	2.21	2.22	2.24	2.31
1ES 1727+502	2.52	2.52	2.52	2.54	2.58
PKS 0548-322	2.44	2.44	2.45	2.51	2.58
BL Lacertae	3.29	3.29	3.30	3.33	3.39
PKS 2005-489	2.77	2.77	2.79	2.85	2.91
RGB J0152+017	2.47	2.47	2.48	2.56	2.63
1ES 1741+196	?	?	?	?	?
SHBL J001355.9-185406	2.81	2.81	2.84	2.94	3.01
W Comae	3.17	3.17	3.20	3.31	3.38
1ES 1312-423	2.17	2.17	2.21	2.34	2.40
VER J0521+211	2.79	2.79	2.82	2.93	3.00
PKS 2155-304	2.81	2.81	2.86	3.00	3.05
B3 2247+381	2.60	2.60	2.64	2.74	2.80
RGB J0710+591	1.89	1.89	1.96	2.12	2.16
H 1426+428	2.85	2.85	2.89	3.01	3.08
1ES 1215+303	2.75	2.75	2.81	2.97	3.03
1ES 1215+303	2.35	2.35	2.40	2.51	2.55
RX J1136.5+6737	?	?	?	?	?
1ES 0806+524	2.70	2.70	2.77	2.93	3.00
1ES 0229+200	0.61	0.62	1.20	1.43	1.26
1RXS J101015.9-311909	2.20	2.20	2.29	2.45	2.49
H 2356-309	2.05	2.05	2.17	2.35	2.40
RX J0648.7+1516	3.45	3.45	3.55	3.71	3.77
1ES 1218+304	1.97	1.97	2.13	2.31	2.34
1ES 1101-232	1.72	1.73	1.96	2.13	2.13
1ES 0347-121	1.87	1.87	2.11	2.28	2.28
RBS 0413	1.88	1.89	2.07	2.28	2.32
RBS 0723	?	?	?	?	?
1ES 1011+496	2.90	2.90	3.06	3.22	3.26
MS 1221.8+2452	?	?	?	?	?
PKS 0301-243	2.93	2.93	3.27	3.46	3.49
1ES 0414+009	1.65	1.65	2.12	2.26	2.25
S5 0716+714	1.60	1.61	2.07	2.22	2.22
1ES 0502+675	?	?	?	?	?
PKS 1510-089	4.02	4.02	4.33	4.45	4.48
3C 66A	1.53	1.54	2.31	2.40	2.39
PKS 1222+216	2.46	2.46	2.79	2.87	2.89
1ES 0647+250	?	?	?	?	?
PG 1553+113	0.98	1.09	2.52	2.30	2.16
3C 279	2.05	2.06	2.71	2.74	2.73
PKS 1424+240	≤ 0.44	≤ 0.50	≤ 1.66	≤ 1.61	≤ 1.56

TABLE IV: Blazars considered in the Table III. For each of them (first column), the deabsorbed value Γ_{em} is reported for different deabsorbing situations. The second column concerns deabsorption according to conventional physics, using the EBL model of FRV. The subsequent columns pertain to the photon-ALP oscillation scenario with the EBL still described by the model of FRV, and report the values of Γ_{em} for different choices of our benchmark values of the model parameter ξ and for $L_{\text{dom}} = 4 \text{ Mpc}$. The total error is the same as for Γ_{obs} and reported in the Table III (for more details see text). Sources with question marks lack information to perform our analysis and are discarded. For PKS 1424+240 only a lower limit for its z exists in the literature: thus, it is neglected in our analysis.

Source	$\Gamma_{\text{em}}^{\text{CP}}$	$\Gamma_{\text{em}}^{\text{ALP}}$			
		$\xi = 0.1$	$\xi = 0.5$	$\xi = 1$	$\xi = 5$
3C 66B	3.00	3.00	3.01	3.01	3.04
Mrk 421	2.05	2.05	2.05	2.07	2.10
Mrk 501	2.54	2.54	2.54	2.57	2.60
1ES 2344+514	2.71	2.71	2.72	2.76	2.79
Mrk 180	3.07	3.07	3.08	3.12	3.14
1ES 1959+650	2.46	2.46	2.48	2.52	2.55
1ES 1959+650	2.32	2.32	2.33	2.38	2.41
AP LIB	2.21	2.21	2.23	2.28	2.31
1ES 1727+502	2.52	2.52	2.53	2.56	2.58
PKS 0548-322	2.44	2.44	2.48	2.56	2.58
BL Lacertae	3.29	3.29	3.31	3.37	3.39
PKS 2005-489	2.77	2.77	2.82	2.89	2.92
RGB J0152+017	2.47	2.47	2.53	2.60	2.63
1ES 1741+196	?	?	?	?	?
SHBL J001355.9-185406	2.81	2.81	2.90	2.99	3.01
W Comae	3.17	3.17	3.27	3.36	3.38
1ES 1312-423	2.17	2.17	2.30	2.38	2.40
VER J0521+211	2.79	2.79	2.89	2.98	3.00
PKS 2155-304	2.81	2.81	2.95	3.03	3.05
B3 2247+381	2.60	2.60	2.71	2.78	2.80
RGB J0710+591	1.89	1.89	2.07	2.15	2.16
H 1426+428	2.85	2.85	2.97	3.06	3.08
1ES 1215+303	2.75	2.75	2.92	3.01	3.03
1ES 1215+303	2.35	2.35	2.47	2.54	2.56
RX J1136.5+6737	?	?	?	?	?
1ES 0806+524	2.70	2.71	2.88	2.98	3.00
1ES 0229+200	0.61	0.65	1.41	1.36	1.25
1RXS J101015.9-311909	2.20	2.20	2.41	2.48	2.49
H 2356-309	2.05	2.06	2.30	2.38	2.40
RX J0648.7+1516	3.45	3.45	3.67	3.75	3.77
1ES 1218+304	1.97	1.97	2.27	2.33	2.34
1ES 1101-232	1.72	1.73	2.10	2.14	2.13
1ES 0347-121	1.87	1.88	2.26	2.29	2.28
RBS 0413	1.88	1.89	2.24	2.31	2.32
RBS 0723	?	?	?	?	?
1ES 1011+496	2.90	2.90	3.19	3.25	3.26
MS 1221.8+2452	?	?	?	?	?
PKS 0301-243	2.93	2.94	3.43	3.48	3.49
1ES 0414+009	1.65	1.67	2.25	2.26	2.25
S5 0716+714	1.60	1.62	2.20	2.22	2.22
1ES 0502+675	?	?	?	?	?
PKS 1510-089	4.02	4.03	4.43	4.47	4.48
3C 66A	1.53	1.58	2.40	2.39	2.39
PKS 1222+216	2.46	2.48	2.86	2.88	2.89
1ES 0647+250	?	?	?	?	?
PG 1553+113	0.98	1.42	2.38	2.22	2.16
3C 279	2.05	2.13	2.74	2.74	2.73
PKS 1424+240	≤ 0.44	≤ 0.70	≤ 1.63	≤ 1.58	≤ 1.56

TABLE V: Same as Table IV, but with $L_{\text{dom}} = 10$ Mpc.

Source	$K_{\text{em}}^{\text{CP}} [\text{cm}^{-2} \text{s}^{-1} \text{TeV}^{-1}]$	$K_{\text{em}}^{\text{ALP}} [\text{cm}^{-2} \text{s}^{-1} \text{TeV}^{-1}]$	
		$L_{\text{dom}} = 4 \text{ Mpc}$	$L_{\text{dom}} = 10 \text{ Mpc}$
3C 66B	$1.99 \cdot 10^{-11}$	$2.13 \cdot 10^{-11}$	$2.32 \cdot 10^{-11}$
Mrk 421	$7.51 \cdot 10^{-10}$	$8.27 \cdot 10^{-10}$	$9.18 \cdot 10^{-10}$
Mrk 501	$1.80 \cdot 10^{-10}$	$2.00 \cdot 10^{-10}$	$2.23 \cdot 10^{-10}$
1ES 2344+514	$6.83 \cdot 10^{-11}$	$7.77 \cdot 10^{-11}$	$8.80 \cdot 10^{-11}$
Mrk 180	$5.82 \cdot 10^{-11}$	$6.64 \cdot 10^{-11}$	$7.52 \cdot 10^{-11}$
1ES 1959+650	$1.14 \cdot 10^{-10}$	$1.31 \cdot 10^{-10}$	$1.49 \cdot 10^{-10}$
1ES 1959+650	$7.62 \cdot 10^{-11}$	$8.75 \cdot 10^{-11}$	$9.94 \cdot 10^{-11}$
AP LIB	?	?	?
1ES 1727+502	$1.29 \cdot 10^{-11}$	$1.51 \cdot 10^{-11}$	$1.72 \cdot 10^{-11}$
PKS 0548-322	$1.50 \cdot 10^{-11}$	$1.81 \cdot 10^{-11}$	$2.07 \cdot 10^{-11}$
BL Lacertae	$8.83 \cdot 10^{-10}$	$1.06 \cdot 10^{-9}$	$1.21 \cdot 10^{-9}$
PKS 2005-489	$4.84 \cdot 10^{-11}$	$5.86 \cdot 10^{-11}$	$6.70 \cdot 10^{-11}$
RGB J0152+017	$2.87 \cdot 10^{-11}$	$3.53 \cdot 10^{-11}$	$4.02 \cdot 10^{-11}$
1ES 1741+196	?	?	?
SHBL J001355.9-185406	$1.12 \cdot 10^{-11}$	$1.42 \cdot 10^{-11}$	$1.60 \cdot 10^{-11}$
W Comae	$1.03 \cdot 10^{-10}$	$1.32 \cdot 10^{-10}$	$1.47 \cdot 10^{-10}$
1ES 1312-423	$9.03 \cdot 10^{-12}$	$1.17 \cdot 10^{-11}$	$1.32 \cdot 10^{-11}$
VER J0521+211	$9.39 \cdot 10^{-11}$	$1.21 \cdot 10^{-10}$	$1.33 \cdot 10^{-10}$
PKS 2155-304	$2.32 \cdot 10^{-10}$	$3.04 \cdot 10^{-10}$	$3.35 \cdot 10^{-10}$
B3 2247+381	$2.77 \cdot 10^{-11}$	$3.58 \cdot 10^{-11}$	$3.86 \cdot 10^{-11}$
RGB J0710+591	$2.49 \cdot 10^{-11}$	$3.32 \cdot 10^{-11}$	$3.66 \cdot 10^{-11}$
H 1426+428	$2.86 \cdot 10^{-10}$	$3.76 \cdot 10^{-10}$	$4.06 \cdot 10^{-10}$
1ES 1215+303	$4.38 \cdot 10^{-11}$	$5.81 \cdot 10^{-11}$	$6.30 \cdot 10^{-11}$
1ES 1215+303	$5.12 \cdot 10^{-11}$	$6.64 \cdot 10^{-11}$	$6.96 \cdot 10^{-11}$
RX J1136.5+6737	?	?	?
1ES 0806+524	$3.76 \cdot 10^{-11}$	$5.03 \cdot 10^{-11}$	$5.41 \cdot 10^{-11}$
1ES 0229+200	$4.04 \cdot 10^{-12}$	$1.21 \cdot 10^{-11}$	$1.50 \cdot 10^{-11}$
1RXS J101015.9-311909	$1.51 \cdot 10^{-11}$	$2.03 \cdot 10^{-11}$	$2.17 \cdot 10^{-11}$
H 2356-309	$2.70 \cdot 10^{-11}$	$3.66 \cdot 10^{-11}$	$3.80 \cdot 10^{-11}$
RX J0648.7+1516	$6.83 \cdot 10^{-11}$	$9.27 \cdot 10^{-11}$	$9.45 \cdot 10^{-11}$
1ES 1218+304	$9.04 \cdot 10^{-11}$	$1.23 \cdot 10^{-10}$	$1.24 \cdot 10^{-10}$
1ES 1101-232	$4.35 \cdot 10^{-11}$	$6.26 \cdot 10^{-11}$	$6.38 \cdot 10^{-11}$
1ES 0347-121	$4.37 \cdot 10^{-11}$	$6.35 \cdot 10^{-11}$	$6.45 \cdot 10^{-11}$
RBS 0413	$3.16 \cdot 10^{-11}$	$4.41 \cdot 10^{-11}$	$4.52 \cdot 10^{-11}$
RBS 0723	?	?	?
1ES 1011+496	$1.43 \cdot 10^{-10}$	$1.92 \cdot 10^{-10}$	$1.89 \cdot 10^{-10}$
MS 1221.8+2452	?	?	?
PKS 0301-243	$3.95 \cdot 10^{-11}$	$5.47 \cdot 10^{-11}$	$5.32 \cdot 10^{-11}$
1ES 0414+009	$2.62 \cdot 10^{-11}$	$3.51 \cdot 10^{-11}$	$3.36 \cdot 10^{-11}$
S5 0716+714	$6.96 \cdot 10^{-10}$	$9.06 \cdot 10^{-10}$	$8.63 \cdot 10^{-10}$
1ES 0502+675	?	?	?
PKS 1510-089	$7.75 \cdot 10^{-11}$	$9.87 \cdot 10^{-11}$	$9.37 \cdot 10^{-11}$
3C 66A	$2.98 \cdot 10^{-10}$	$4.01 \cdot 10^{-10}$	$3.81 \cdot 10^{-10}$
PKS 1222+216	$1.80 \cdot 10^{-9}$	$2.09 \cdot 10^{-9}$	$1.98 \cdot 10^{-9}$
1ES 0647+250	?	?	?
PG 1553+113	$4.73 \cdot 10^{-10}$	$7.86 \cdot 10^{-10}$	$6.83 \cdot 10^{-10}$
3C 279	$2.30 \cdot 10^{-9}$	$2.28 \cdot 10^{-9}$	$2.19 \cdot 10^{-9}$
PKS 1424+240	$\geq 1.92 \cdot 10^{-10}$	$\geq 2.15 \cdot 10^{-10}$	$\geq 2.06 \cdot 10^{-10}$

TABLE VI: Blazars considered in the Table III. For each of them (first column), the deabsorbed value K_{em} is reported for different deabsorbing situations. The second column concerns deabsorption according to conventional physics, using the EBL model of FRV. The subsequent columns pertain to the photon-ALP oscillation scenario with the EBL still described by the model of FRV, and report the values of K_{em} for different choices of our benchmark values of the model parameter L_{dom} and for $\xi = 0.5$ – which are the best values of the model (for more details see text). Sources with question marks lack information to perform our analysis and are discarded. For PKS 1424+240 only a lower limit for its z exists in the literature: thus, it is neglected in our analysis.

Source	$F_{\text{em},\Delta E}^{\text{CP}} [\text{cm}^{-2} \text{s}^{-1}]$	$F_{\text{em},\Delta E}^{\text{ALP}} [\text{cm}^{-2} \text{s}^{-1}]$	
		$L_{\text{dom}} = 4 \text{ Mpc}$	$L_{\text{dom}} = 10 \text{ Mpc}$
3C 66B	$1.75 \cdot 10^{-11}$	$1.87 \cdot 10^{-11}$	$2.03 \cdot 10^{-11}$
Mrk 421	$4.65 \cdot 10^{-10}$	$5.12 \cdot 10^{-10}$	$5.69 \cdot 10^{-10}$
Mrk 501	$5.46 \cdot 10^{-11}$	$6.06 \cdot 10^{-11}$	$6.76 \cdot 10^{-11}$
1ES 2344+514	$2.80 \cdot 10^{-11}$	$3.19 \cdot 10^{-11}$	$3.61 \cdot 10^{-11}$
Mrk 180	$2.09 \cdot 10^{-11}$	$2.38 \cdot 10^{-11}$	$2.70 \cdot 10^{-11}$
1ES 1959+650	$3.88 \cdot 10^{-11}$	$4.45 \cdot 10^{-11}$	$5.05 \cdot 10^{-11}$
1ES 1959+650	$2.74 \cdot 10^{-11}$	$3.14 \cdot 10^{-11}$	$3.56 \cdot 10^{-11}$
AP LIB	?	?	?
1ES 1727+502	$1.11 \cdot 10^{-11}$	$1.29 \cdot 10^{-11}$	$1.48 \cdot 10^{-11}$
PKS 0548-322	$2.33 \cdot 10^{-12}$	$2.79 \cdot 10^{-12}$	$3.12 \cdot 10^{-12}$
BL Lacertae	$4.41 \cdot 10^{-10}$	$5.31 \cdot 10^{-10}$	$6.06 \cdot 10^{-10}$
PKS 2005-489	$5.94 \cdot 10^{-12}$	$7.14 \cdot 10^{-12}$	$7.99 \cdot 10^{-12}$
RGB J0152+017	$4.24 \cdot 10^{-12}$	$5.17 \cdot 10^{-12}$	$5.70 \cdot 10^{-12}$
1ES 1741+196	?	?	?
SHBL J001355.9-185406	$7.34 \cdot 10^{-13}$	$9.09 \cdot 10^{-13}$	$9.70 \cdot 10^{-13}$
W Comae	$1.26 \cdot 10^{-11}$	$1.59 \cdot 10^{-11}$	$1.73 \cdot 10^{-11}$
1ES 1312-423	$1.42 \cdot 10^{-12}$	$1.76 \cdot 10^{-12}$	$1.82 \cdot 10^{-12}$
VER J0521+211	$1.95 \cdot 10^{-11}$	$2.48 \cdot 10^{-11}$	$2.69 \cdot 10^{-11}$
PKS 2155-304	$5.38 \cdot 10^{-11}$	$6.93 \cdot 10^{-11}$	$7.44 \cdot 10^{-11}$
B3 2247+381	$1.10 \cdot 10^{-11}$	$1.43 \cdot 10^{-11}$	$1.55 \cdot 10^{-11}$
RGB J0710+591	$4.79 \cdot 10^{-12}$	$5.92 \cdot 10^{-12}$	$5.81 \cdot 10^{-12}$
H 1426+428	$2.04 \cdot 10^{-11}$	$2.66 \cdot 10^{-11}$	$2.82 \cdot 10^{-11}$
1ES 1215+303	$4.49 \cdot 10^{-12}$	$5.78 \cdot 10^{-12}$	$5.96 \cdot 10^{-12}$
1ES 1215+303	$3.92 \cdot 10^{-11}$	$5.17 \cdot 10^{-11}$	$5.58 \cdot 10^{-11}$
RX J1136.5+6737	?	?	?
1ES 0806+524	$2.86 \cdot 10^{-12}$	$3.71 \cdot 10^{-12}$	$3.78 \cdot 10^{-12}$
1ES 0229+200	$7.93 \cdot 10^{-12}$	$6.06 \cdot 10^{-12}$	$4.84 \cdot 10^{-12}$
1RXS J101015.9-311909	$3.10 \cdot 10^{-12}$	$3.94 \cdot 10^{-12}$	$3.89 \cdot 10^{-12}$
H 2356-309	$6.02 \cdot 10^{-12}$	$7.83 \cdot 10^{-12}$	$7.75 \cdot 10^{-12}$
RX J0648.7+1516	$9.78 \cdot 10^{-12}$	$1.32 \cdot 10^{-11}$	$1.33 \cdot 10^{-11}$
1ES 1218+304	$2.85 \cdot 10^{-11}$	$3.67 \cdot 10^{-11}$	$3.56 \cdot 10^{-11}$
1ES 1101-232	$1.17 \cdot 10^{-11}$	$1.36 \cdot 10^{-11}$	$1.22 \cdot 10^{-11}$
1ES 0347-121	$9.46 \cdot 10^{-12}$	$1.10 \cdot 10^{-11}$	$9.86 \cdot 10^{-12}$
RBS 0413	$4.64 \cdot 10^{-12}$	$5.79 \cdot 10^{-12}$	$5.38 \cdot 10^{-12}$
RBS 0723	?	?	?
1ES 1011+496	$3.93 \cdot 10^{-11}$	$5.30 \cdot 10^{-11}$	$5.24 \cdot 10^{-11}$
MS 1221.8+2452	?	?	?
PKS 0301-243	$3.31 \cdot 10^{-12}$	$4.10 \cdot 10^{-12}$	$3.79 \cdot 10^{-12}$
1ES 0414+009	$7.70 \cdot 10^{-12}$	$8.49 \cdot 10^{-12}$	$7.76 \cdot 10^{-12}$
S5 0716+714	$1.69 \cdot 10^{-10}$	$1.90 \cdot 10^{-10}$	$1.75 \cdot 10^{-10}$
1ES 0502+675	?	?	?
PKS 1510-089	$2.04 \cdot 10^{-11}$	$2.77 \cdot 10^{-11}$	$2.69 \cdot 10^{-11}$
3C 66A	$3.62 \cdot 10^{-11}$	$3.58 \cdot 10^{-11}$	$3.29 \cdot 10^{-11}$
PKS 1222+216	$9.36 \cdot 10^{-10}$	$1.28 \cdot 10^{-9}$	$1.26 \cdot 10^{-9}$
1ES 0647+250	?	?	?
PG 1553+113	$1.50 \cdot 10^{-10}$	$7.59 \cdot 10^{-11}$	$7.23 \cdot 10^{-11}$
3C 279	$9.19 \cdot 10^{-10}$	$1.14 \cdot 10^{-9}$	$1.11 \cdot 10^{-9}$
PKS 1424+240	$\geq 5.65 \cdot 10^{-11}$	$\geq 4.20 \cdot 10^{-11}$	$\geq 4.05 \cdot 10^{-11}$

TABLE VII: Blazars considered in the Table III. For each of them (first column), the deabsorbed value $F_{\text{em},\Delta E}$ is reported for different deabsorbing situations. The second column concerns deabsorption according to conventional physics, using the EBL model of FRV. The subsequent columns pertain to the photon-ALP oscillation scenario with the EBL still described by the model of FRV, and report the values of $F_{\text{em},\Delta E}$ for different choices of our benchmark values of the model parameter L_{dom} and for $\xi = 0.5$ – which are the best values of the model (for more details see text). Sources with question marks lack information to perform our analysis and are discarded. For PKS 1424+240 only a lower limit for its z exists in the literature: thus, it is neglected in our analysis.